

# Interacting holes in Si and Ge double quantum dots: from a multiband approach to an effective-spin picture

Andrea Secchi,<sup>\*</sup> Laura Bellentani, Andrea Bertoni, and Filippo Troiani  
*Centro S3, CNR-Istituto di Nanoscienze, I-41125 Modena, Italy*  
 (Dated: April 1, 2024)

The states of two electrons in tunnel-coupled semiconductor quantum dots can be described in terms of a two-spin Hamiltonian with an isotropic Heisenberg interaction. A similar description does not apply in the case of holes due to their multiband character and spin-orbit coupling, which introduces a strong anisotropy in the angular-momentum space and mixes orbital and spin degrees of freedom. Here we investigate two-hole states in coupled Si and Ge quantum dots within a 6-band  $\mathbf{k}\cdot\mathbf{p}$  and Configuration-Interaction approach. We integrate and interpret the numerical results by means of an effective 4-band Hubbard model, which provides general expressions for the two-hole eigenstates. The spin-orbit mixing in the single- and two-hole states is quantified via the computation of the linear entropy of the reduced spin density operator. We find that the ground state and first excited multiplet of the two-hole system are, respectively, a singlet and a triplet; however, differently from the one-band case, they are characterized by a combination of states belonging to different  $J$  subspaces, with dominant contributions coming respectively from even and odd values of  $J$ . Finally, by combining our numerical results with the effective model, we illustrate a pseudospin-1/2 description of the single-hole states which accounts for the main features of the lowest two-hole states in the regime of weak spin-orbit entanglement.

## I. INTRODUCTION

Semiconductor quantum dots (QDs) and double quantum dots (DQDs)<sup>1–3</sup> represent the solid-state analogues of atoms and biatomic molecules, respectively. Unlike in the case of atoms, the main QD features, such as the shape of the confining potential and the interdot coupling, can be widely tuned by means of electrostatic gates. Besides, the properties of the confined particles in QDs are affected and diversified by the host semiconductor and its band structure.

From a technological viewpoint, one of the most relevant applications of QDs is represented by the implementation of spin qubits<sup>4</sup>. In this perspective, Si/Ge nanostructures seem to represent ideal building blocks. In fact, both semiconductors present a reduced hyperfine interaction, due to the natural abundance of nonmagnetic isotopes ( $> 95\%$  and  $> 92\%$  for Si and Ge, respectively) and to the possibility of isotopically purifying the samples<sup>5,6</sup>. Moreover, the availability of well-established industrial technologies for the production of Si/Ge nanostructures, such as metal-oxide-semiconductor devices, possibly represents a crucial asset towards scalability<sup>7,8</sup>.

Although a great deal of work has been performed on conduction-band Si QDs<sup>9–18</sup>, the implementation of hole QDs has recently attracted considerable interest for quantum applications<sup>6,19–27</sup>. One reason is that the valence band of both Si and Ge does not display the 6-fold valley degeneracy that characterizes the conduction band<sup>28</sup>, which represents an unwanted additional degree of freedom. Furthermore, the valence band is generated by the hybridization of  $p$  atomic orbitals<sup>29</sup>, which have nodes at the atomic nuclei, therefore the residual hyperfine interaction affects the hole states only weakly. In the context of hole implementation of qubits, germanium has some advantages with respect to silicon<sup>6,22–26</sup>: because of

its smaller hole effective mass, Ge holes can tunnel more easily between QDs, which do not need to be excessively small or close to each other.

The valence band of Si and Ge is made of three distinct subbands, having their maximum at the  $\Gamma$  point, namely the heavy-hole, the light-hole, and the split-off bands<sup>29,30</sup>. Each subband is doubly degenerate at zero magnetic field (Kramers degeneracy), and the heavy- and light-hole bands are degenerate at  $\Gamma$ , while the split-off bands lie at a higher energy that is equal to the spin-orbit parameter. This scenario results from a strong spin-orbit coupling between the hole spins and orbital angular momenta, which can be exploited for efficient spin manipulation through electric-dipole spin resonance<sup>23,31</sup>. The much weaker spin-orbit coupling acting in the conduction band makes the implementation of this concept more challenging for electrons<sup>32</sup>. To exploit these advantages brought forward by the use of holes, we need to carefully understand the implications for quantum computing of the Si and Ge valence bands' structure close to the  $\Gamma$  point.

The presence of distinct subbands also complicates the character of two-particle states in coupled quantum dots. In the single-band case, interdot tunneling induces a hybridization of the single-dot orbitals. In the case of weak tunneling and identical dots, the single-particle spatial wave functions can be approximately identified with symmetric and antisymmetric combinations of single-dot orbitals. The lowest two-particle eigenstates result from the interplay between tunneling and Coulomb interactions and, for weak spin-orbit coupling, can be assigned well-defined values of the total spin  $S$ . In particular, the ground and first excited states respectively correspond to a spin singlet ( $S = 0$ ) and triplet ( $S = 1$ )<sup>33</sup>.

In the multiband case, the single-dot ground state is

the combination of different band terms (i.e., different Bloch states), each of which might be coupled to a different orbital envelope function. For tunnel-coupled quantum dots, this results in a richer and more complicated picture with respect to the one outlined in the single-band case. The lowest molecular orbitals are determined by the competition between different excitations, associated to interdot and band degrees of freedom. In particular geometries, the interplay between the confinement potential and spin-orbit coupling can lead to the appearance of anomalous features, like the vanishing of the tunneling energy at finite interdot distances, and the related vanishing of the singlet-triplet splitting<sup>2,34–36</sup>.

The purpose of this work is to elucidate the effect of the multiband structure of the valence band on the single- and two-hole wave functions of Si and Ge confined states. We consider the case of horizontal electrostatically-defined DQDs, where tunneling takes place within a given quantum well and across a smooth barrier, modulated by top gates. We determine the single- and two-hole states for a model DQD potential within a six-band  $\mathbf{k} \cdot \mathbf{p}$  envelope-function approach combined with the Configuration-Interaction (CI) scheme for the diagonalization of the two-hole interacting Hamiltonian. The numerical results are taken as the benchmark and the starting point for an effective representation in terms of an analytical model. The latter is inspired by the Hubbard model, where the two QDs play the role of the atomic sites, and two Kramers-degenerate spin-orbital states for each QD are included. Crucially, we take into account the band structure of each of these spin-orbitals (simplified to four bands), which allows to obtain analytical expressions for the single- and two-hole eigenstates of the model, from which it is possible to analyze their spin content as well as their dependence on the single-dot orbital wave functions. We find that the two-hole states are non-trivial mixtures of spinors with different values of the total spin  $J$  and its third component  $M$ . The predictions of the model are checked against the numerical modeling and reveal a very good agreement; this is our first main result. The band mixing occurring in the two-hole states, that we have unveiled, needs to be carefully taken into account when devising algorithms based on the spin-Pauli blockade in Si/Ge DQD hole qubits.

Our second main result follows from the numerical calculations of the linear entropies associated with the reduced spin density matrices of the lowest eigenstates of the single- and two-hole systems. These calculations reveal that spin-orbit entanglement is rather weak in these systems; this implies that the single-hole orbital wave functions corresponding to different bands are ap-

proximately parallel (i.e., they differ by a multiplicative constant). This allows us to simplify the results of the Hubbard model, and to derive a simpler description of the single- and two-hole states in terms of pseudospin-1/2 states. This demonstrates that linear entropies are a powerful tool for the analysis and the derivation of effective models for multiband systems.

The rest of this article is organized as follows. In Section II, we discuss the single-hole states, from the method for their calculation, to the theoretical tools for their characterization and to the numerical results. In Section III, we do the same for the two-hole states. In Section IV we discuss our analytical 4-band Hubbard model, and we compare its predictions to the numerical results. In Section V, based on the strength of the above numerical results, we introduce the approximation of neglecting the spin-orbit entanglement, which allows to obtain from the Hubbard model a simpler pseudospin-1/2 representation of the single- and two-hole states. Finally, in Section VI we summarize the main findings of this work. Further technical details related to the comparison between the numerical results and the 4-band Hubbard model are reported in Appendix A.

## II. SINGLE-HOLE STATES

### A. Method

#### 1. Diagonalization of the single-hole Hamiltonian

For the calculation of the single-hole states in Si and Ge in the presence of a confinement potential, we adopt the Luttinger-Kohn envelope-function approach<sup>37</sup>. As a first step, the kinetic-energy operator for the electronic states close to the top of the valence bands (which occurs at the  $\Gamma$  point in both Si and Ge) is represented by a  $\mathbf{k} \cdot \mathbf{p}$  Hamiltonian matrix, which we denote as  $H_{\mathbf{k} \cdot \mathbf{p}}$ . This Hamiltonian acts on vectors, each component of which corresponds to a Bloch state with crystal momentum  $\Gamma \equiv \mathbf{0}$ . In the cases of Si and Ge, the relevant Bloch states for the valence bands are built from  $p$ -type atomic orbitals<sup>29,38</sup>, carrying an angular momentum  $l = 1$ . Combining this with the electron  $s = 1/2$  spin, one can write the Bloch basis set at  $\Gamma$  as a quartet of states with  $j = 3/2$  and a doublet of states with  $j = 1/2$ . The  $j = 3/2$  quartet generates the heavy- ( $m = \pm 3/2$ ) and light-hole ( $m = \pm 1/2$ ) bands, while the  $j = 1/2$  doublet generates the spin-orbit split-off bands. The  $\mathbf{k} \cdot \mathbf{p}$  Hamiltonian is therefore a  $6 \times 6$  matrix. In the  $\{|\frac{3}{2}, \frac{3}{2}\rangle, |\frac{3}{2}, \frac{1}{2}\rangle, |\frac{3}{2}, -\frac{1}{2}\rangle, |\frac{3}{2}, -\frac{3}{2}\rangle, |\frac{1}{2}, \frac{1}{2}\rangle, |\frac{1}{2}, -\frac{1}{2}\rangle\}$  basis, it reads as<sup>29,30</sup>

$$H_{\mathbf{k},\mathbf{p}} = \begin{pmatrix} P+Q & -S & R & 0 & -\frac{1}{\sqrt{2}}S & \sqrt{2}R \\ -S^* & P-Q & 0 & R & -\sqrt{2}Q & \sqrt{\frac{3}{2}}S \\ R^* & 0 & P-Q & S & \sqrt{\frac{3}{2}}S^* & \sqrt{2}Q \\ 0 & R^* & S^* & P+Q & -\sqrt{2}R^* & -\frac{1}{\sqrt{2}}S^* \\ -\frac{1}{\sqrt{2}}S^* & -\sqrt{2}Q & \sqrt{\frac{3}{2}}S & -\sqrt{2}R & P+\Delta & 0 \\ \sqrt{2}R^* & \sqrt{\frac{3}{2}}S^* & \sqrt{2}Q & -\frac{1}{\sqrt{2}}S & 0 & P+\Delta \end{pmatrix}, \quad (1)$$

where we have chosen the sign such that the hole effective masses are positive, and where

$$P = \frac{\hbar^2}{2m_0}\gamma_1(k_x^2 + k_y^2 + k_z^2), \quad (2)$$

$$Q = \frac{\hbar^2}{2m_0}\gamma_2(k_x^2 + k_y^2 - 2k_z^2), \quad (3)$$

$$R = \frac{\hbar^2}{2m_0}\sqrt{3}[-\gamma_3(k_x^2 - k_y^2) + 2i\gamma_2k_xk_y], \quad (4)$$

$$S = \frac{\hbar^2}{2m_0}2\sqrt{3}\gamma_3(k_x - ik_y)k_z. \quad (5)$$

The above expression of  $H_{\mathbf{k},\mathbf{p}}$  applies when the following correspondence holds between the reference and crystallographic axes<sup>39</sup>:  $\hat{\mathbf{x}} \parallel [110]$ ,  $\hat{\mathbf{y}} \parallel [\bar{1}10]$ , and  $\hat{\mathbf{z}} \parallel [001]$ . The Luttinger parameters are  $\{\gamma_1, \gamma_2, \gamma_3\} = \{4.285, 0.339, 1.446\}$  for Si, and  $\{\gamma_1, \gamma_2, \gamma_3\} = \{13.38, 4.24, 5.69\}$  for Ge; the spin-orbit parameter is  $\Delta = 44$  meV for Si, and  $\Delta = 290$  meV for Ge.

In the presence of an external electrostatic potential  $V(\mathbf{r})$  that varies smoothly over the length scale of the lattice, the effective Hamiltonian for the low-energy hole states is given by the Luttinger-Kohn (LK) expression,

$$H_{\text{LK}} = H_{\mathbf{k},\mathbf{p}} + \text{diag}[V(\mathbf{r})], \quad (6)$$

where the external potential is added to the diagonal elements of  $H_{\mathbf{k},\mathbf{p}}$  [Eq. (1)]. The solution of the matrix Schrödinger equation determined by  $H_{\text{LK}}$  yields eigenvectors whose  $\mathbf{r}$ -dependent components are the envelope functions: we denote them as  $\psi_{\alpha,b}(\mathbf{r})$ , where  $\alpha$  is the eigenstate index and  $b \equiv (j, m)$  distinguishes the 6 components (bands). The total eigenstates, including the microscopic (Bloch) parts, are written in the  $\mathbf{r}$ -representation as

$$|\psi_{\alpha}(\mathbf{r})\rangle = \sum_b \psi_{\alpha,b}(\mathbf{r})|\varepsilon_b^+(\mathbf{r})\rangle, \quad (7)$$

where

$$|\varepsilon_b^+(\mathbf{r})\rangle = \frac{1}{\sqrt{N_a}} \sum_{\mathbf{R}_k} (-1)^k \sum_{\xi, s_z} S_{b,\xi,s_z} \phi_{p\xi}(\mathbf{r} - \mathbf{R}_k) |s_z\rangle \quad (8)$$

is the Bloch state<sup>29,38</sup> for band  $b$ , that combines  $p$ -atomic orbitals ( $\phi_{p\xi}$ , with  $\xi \in \{x, y, z\}$ ) centered at all the  $N_a$  atomic positions  $\mathbf{R}_k$  of the crystal (where  $k \in \{0, 1\}$  labels the two atoms in each unit cell) with spin states ( $s_z = \pm 1/2$ ), through the Clebsch-Gordan coefficients  $S_{b,\xi,s_z}$ .

In this work, we focus on prototypical double quantum dots (DQDs), defined within a Si or Ge quantum well by means of electrostatic gates. The hole confinement is accounted for by the total potential

$$V(\mathbf{r}) = V_{\text{DQD}}(x) + V_{\text{DQD}}(y) + V_{\parallel}\theta(|z| - L_z/2), \quad (9)$$

where the confinement potentials in the  $(x, y)$  plane are given by

$$V_{\text{DQD}}(x) = \frac{1}{2}\kappa \frac{(x^2 - a^2)^2}{4a^2}, \quad V_{\text{DQD}}(y) = \frac{1}{2}\kappa y^2. \quad (10)$$

The minima of  $V_{\text{DQD}}(x)$  are located at  $x = \pm a$ , and are thus separated by a distance  $D = 2a$ , to which we refer in the following as the *interdot distance*. The height of the interdot barrier is  $V(\mathbf{0}) = \kappa a^2/8$ . For  $|x \mp a| \ll a$ , the confinement along the  $x$  direction is approximately harmonic, with the same spring constant as the one that characterizes the harmonic potential along the  $y$  direction:

$$V_{\text{DQD}}(x) \approx \frac{1}{2}\kappa (x \mp a)^2. \quad (11)$$

Finally, the confinement along  $z$  is provided by a hard-wall potential, with a height  $V_{\parallel}$  that mimics the band offset between the semiconductor and the surrounding insulating materials.

## 2. Characterization of the single-hole states

If we neglect the  $\mathbf{r}$ -dependence of the Bloch states in Eq. (7), we can rewrite the single-hole eigenstates as

$$|\psi_{\alpha}\rangle = \sum_b |\psi_{\alpha,b}\rangle \otimes |b\rangle, \quad (12)$$

where we have decoupled the states  $|\psi_{\alpha,b}\rangle$  defined in the position space, i.e., the envelope functions, from the band states  $|b\rangle$ , which take the place of the Bloch states and, in this picture, can be considered as spinors. Hereinafter, we refer to envelope and band as the *orbital* and *spin* degrees of freedom, respectively.

The occupations of the six bands, whose sum is normalized to 1, are given by:

$$p_{\alpha,b} \equiv \langle \psi_{\alpha,b} | \psi_{\alpha,b} \rangle. \quad (13)$$

The eigenstates  $|\psi_{\alpha}\rangle$  can be also characterized in terms of their spatial symmetries. In the following, we specifically refer to the expectation value of the operator  $\sigma_{yz}$ , which implements a reflection of the orbital states about the  $(y, z)$  plane, and is thus defined by the equation

$$\langle x, y, z | \sigma_{yz} | \psi_{\alpha} \rangle = \langle -x, y, z | \psi_{\alpha} \rangle. \quad (14)$$

In the single-hole states  $|\psi_{\alpha}\rangle$ , orbital and spin degrees of freedom are in general entangled. This means that it is *not* possible to write such states exactly in the factorized form

$$|\psi_{\alpha}^{\text{fact}}\rangle \equiv |\psi_{\alpha,1}\rangle \otimes \sum_b c_{\alpha,b} |b\rangle, \quad (15)$$

with the normalization

$$\langle \psi_{\alpha,1} | \psi_{\alpha,1} \rangle = 1 = \sum_b |c_{\alpha,b}|^2. \quad (16)$$

The state in Eq. (15) is the product of an orbital function  $|\psi_{\alpha,1}\rangle$ , common for all bands, and a spin state  $\sum_b c_{\alpha,b} |b\rangle$ , which is in general a linear combination of the band states.

The true eigenstates of our system actually display band mixing, i.e., different bands are coupled to different orbital functions. In order to investigate such mixing, we first compute the reduced single-spin density matrix:

$$\rho_{\alpha}^{\text{sp}} = \sum_{b,b'} \langle \psi_{\alpha,b'} | \psi_{\alpha,b} \rangle |b\rangle \langle b'|. \quad (17)$$

Then, the entanglement between the orbital (envelope) and spin (band) degrees of freedom is quantified through the linear entropy of the reduced spin state:

$$S_L(\rho_{\alpha}^{\text{sp}}) = 1 - \text{tr}[(\rho_{\alpha}^{\text{sp}})^2] = 1 - \sum_{b,b'} |\langle \psi_{\alpha,b'} | \psi_{\alpha,b} \rangle|^2, \quad (18)$$

which ranges from 0 to 5/6, for increasing spin-orbit correlations and mixing of the density matrix  $\rho_{\alpha}^{\text{sp}}$ ; one has  $S_L(\rho_{\alpha}^{\text{sp}}) = 0$  if and only if the hole state  $|\psi_{\alpha}\rangle$  has the factorized form given in Eq. (15).

In this system, spin-orbit entanglement, i.e.,  $S_L(\rho_{\alpha}^{\text{sp}}) \neq 0$ , is due to two conditions, both of which are necessary. The first condition is the occurrence of band mixing, i.e., the distribution of the population among the different bands. The second condition is that the (unnormalized) orbital states corresponding to

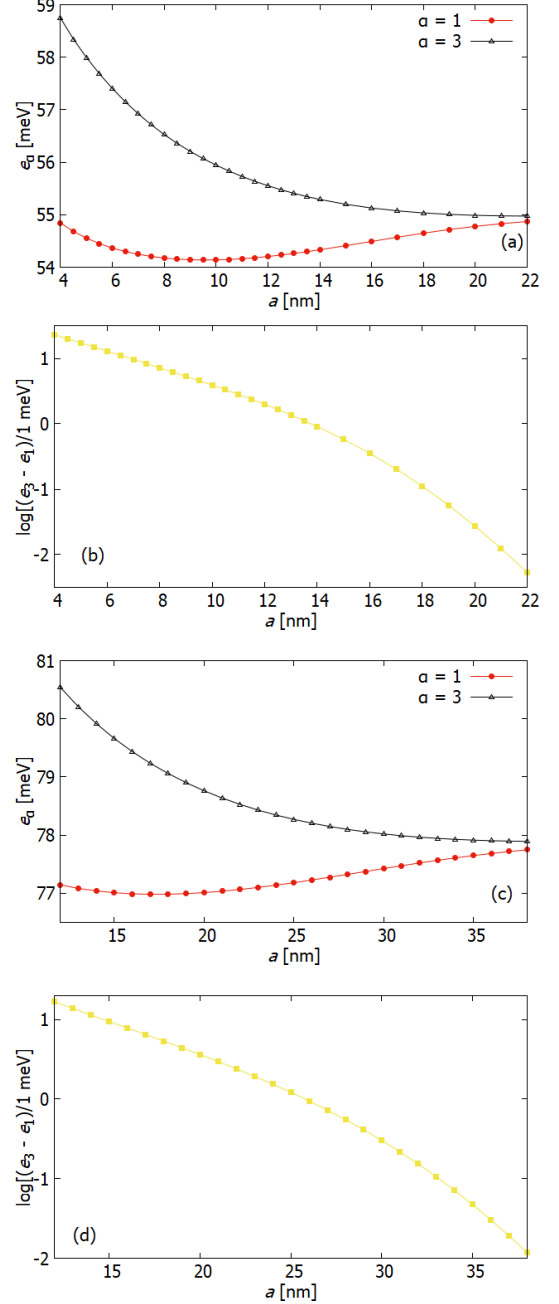


FIG. 1. Energies of the single-hole ground and first-excited states in the (a) Si and (c) Ge double quantum dot, as functions of the half interdot distance  $a = D/2$ . Panels (b) and (d) report the energy difference between these states for silicon and germanium, respectively.

the different bands are not parallel to each other, i.e., that there are no constants  $c_{\alpha,b}$  such that  $|\psi_{\alpha}\rangle$  can be factorized as in Eq. (15).

In order to assess these two contributions, we compare the linear entropy of  $\rho_{\alpha}^{\text{sp}}$  with that of the fully-dephased

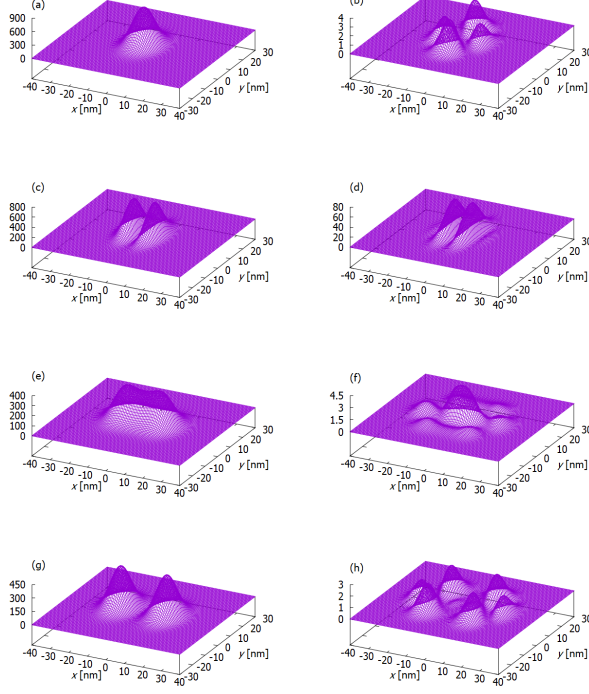


FIG. 2. Profile along the in-plane directions, for  $z = 0$ , of the band-resolved charge density  $\rho_{\alpha,(3/2,m)}^{\text{ch}}(\mathbf{r})$  in the Si dots (arbitrary units). Panels a-d and e-h refer to the representative interdot distances  $D = 8$  nm and  $D = 26$  nm, respectively. a, e:  $(\alpha, m) = (1, 3/2)$ ; b, f:  $(\alpha, m) = (1, -1/2)$ ; c, g:  $(\alpha, m) = (3, 3/2)$ ; d, h:  $(\alpha, m) = (3, -1/2)$ . Since the states with  $\alpha = 2$  and  $\alpha = 4$  are the time-reversal conjugates of  $\alpha = 1$  and  $\alpha = 3$ , respectively, one has  $\rho_{2,(j,m)}^{\text{ch}} = \rho_{1,(j,-m)}^{\text{ch}}$  and  $\rho_{4,(j,m)}^{\text{ch}} = \rho_{3,(j,-m)}^{\text{ch}}$ .

reduced density operator

$$\sigma_{\alpha}^{\text{sp}} = \sum_b \langle \psi_{\alpha,b} | \psi_{\alpha,b} \rangle |b\rangle \langle b|, \quad (19)$$

which is given by

$$S_L(\sigma_{\alpha}^{\text{sp}}) = 1 - \sum_b |\langle \psi_{\alpha,b} | \psi_{\alpha,b} \rangle|^2 \geq S_L(\rho_{\alpha}^{\text{sp}}). \quad (20)$$

The linear entropy  $S_L(\sigma_{\alpha}^{\text{sp}})$  quantifies the band mixing alone, while the difference

$$S_L(\sigma_{\alpha}^{\text{sp}}) - S_L(\rho_{\alpha}^{\text{sp}}) = \sum_b \sum_{b' \neq b} |\langle \psi_{\alpha,b'} | \psi_{\alpha,b} \rangle|^2 \quad (21)$$

singles out the contribution to spin-orbit entanglement resulting from the different spatial dependencies of the orbital states corresponding to different bands. Low values of  $S_L(\rho_{\alpha}^{\text{sp}})$  imply that the state  $|\psi_{\alpha}\rangle$  can be associated with a well-defined (i.e., non-mixed) spin state, either because the hole eigenstate presents a low degree of band mixing [relatively low values of  $S_L(\sigma_{\alpha}^{\text{sp}})$ ], or because the

orbital states corresponding to the different spin components are strongly overlapping [relatively high values of  $S_L(\sigma_{\alpha}^{\text{sp}})$ ].

## B. Numerical results

We investigate the properties of the single-hole states in two Si and Ge horizontally coupled quantum dots, as a function of the interdot coupling.

### 1. Interdot tunneling

Within the present model, the interdot tunneling is tuned by varying the parameter  $a$  in the potential  $V_{\text{DQD}}(x, y)$ . In fact,  $a$  determines the distance  $D = 2a$  between the two potential minima ( $x = \pm a, y = 0$ ) that define the positions of the dots, and the height of the interdot barrier, given by  $V_{\text{DQD}}(0, 0) = \kappa a^2/8$ . Here we define the strength of the confinement in terms of the inter-level energy spacing,  $\kappa = m_0 \omega^2 / \gamma_1$ , with  $\omega = 5 \text{ meV}/\hbar$  for both the Si and the Ge dots. The parameter  $\gamma_1$ , and thus the “effective mass”  $m_0/\gamma_1$ , is different in the two materials, and the ratio between the characteristic length scales is  $l_{\text{Ge}}/l_{\text{Si}} \approx 1.767$ , where  $l \equiv (\hbar \gamma_1 / m_0 \omega)^{1/2}$ . The confinement along the  $z$  direction is induced by a potential well whose depth is given by  $V_{\parallel} = 4.0 \text{ eV}$ .

We are specifically interested in the weak interdot coupling regime, where the energy scale associated to the interdot tunneling is smaller than that associated with the intradot excitations ( $\delta$ ). The lowest energy eigenvalues  $e_{\alpha}$  as functions of  $a$  are shown in Fig. 1 for the cases of Si and Ge. In the absence of an applied magnetic field, each energy level is doubly degenerate (Kramers degeneracy), so  $e_1 = e_2, e_3 = e_4$ , etcetera. The energy difference between the ground doublet and the first excited one decreases (faster than exponentially) as a function of  $a$  and drops below the intradot gap ( $\delta_{\text{Si}} \approx 3.94 \text{ meV}$ ) for  $a \approx 4 \text{ nm}$  in the case of Si. All the considered values of  $a$  correspond to a weak interdot coupling regime in the case of Ge ( $\delta_{\text{Ge}} \approx 4.58 \text{ meV}$ ).

In order to visualize the effect of the interdot tunneling and the degree of orthogonality between the orbitals corresponding to different bands, we plot the profile along the  $xy$  plane of the band-resolved charge density

$$\rho_{\alpha,b}^{\text{ch}}(\mathbf{r}) = |\langle \mathbf{r} | \psi_{\alpha,b} \rangle|^2, \quad (22)$$

for the states  $\alpha = 1$  and  $\alpha = 3$ , and for two representative values of  $D$  (Fig. 2). The overall character of each eigenstate is determined by the dominant heavy-hole contribution  $(j, m) = (3/2, 3/2)$ , which is bonding and anti-bonding for the ground [panels (a, e)] and first excited (c, g) states, respectively. The main light-hole component  $(j, m) = (3/2, -1/2)$  clearly displays a different spatial distribution, with a larger number of nodes (b, d, f, h). In particular, we observe a transition in the excited state:



Si	$ \psi_1\rangle$		$ \psi_3\rangle$	
$a$ [nm]	4	22	4	22
$p_{\alpha,3/2,3/2}$	0.989	0.904	0.895	0.919
$p_{\alpha,3/2,-1/2}$	0.006	0.0801	0.083	0.0643
$\langle\sigma_{yz}\rangle_\alpha$	0.996	1.00	-0.973	-1.00
$S_L(\rho_\alpha^{\text{sp}})$	0.0212	0.0216	0.0480	0.0207
$S_L(\sigma_\alpha^{\text{sp}})$	0.0217	0.0225	0.193	0.0207

TABLE I. Values taken for two representative values of  $a$  of: the largest band occupations  $p_{\alpha,b}$ ; the expectation value of the symmetry operator  $\sigma_{yz}$  (where  $\langle\sigma_{yz}\rangle_\alpha = \langle\psi_\alpha|\sigma_{yz}|\psi_\alpha\rangle$ ); the linear entropy of the spin reduced density operators  $\rho_\alpha^{\text{sp}}$  and  $\sigma_\alpha^{\text{sp}}$ .

at small interdot distances, its heavy- and light- hole spatial distributions (c, d) display a strong resemblance, while at larger distances they are nearly disjointed (g, h). Such transition is captured in the dependence of the linear entropies on  $a$  (see below). We omit the minority contributions to the charge density, which for states  $\alpha = 1$  and  $\alpha = 3$  correspond to  $(j, m) = (3/2, -3/2)$ ,  $(j, m) = (3/2, 1/2)$  and  $j = 1/2$ , as they are very small.

## 2. Band composition, symmetries and spin-orbit correlation

The single-hole states can be characterized in terms of the band composition, of the symmetry of the band components, and of the spin-orbit correlation.

In the case of Si, the ground states  $|\psi_1\rangle$  and  $|\psi_2\rangle$  have a predominant heavy-hole character. At zero magnetic field, the individual eigenstates within each Kramers doublet are not unambiguously defined. In this set of calculations we break the Kramers degeneracy and unambiguously define the eigenstates by including a magnetic field of  $10^{-2}$  T along  $z$ , which is weak enough to avoid mixing between states belonging to different doublets. Therefore, the state  $|\psi_1\rangle$  is characterized by a dominant  $(j, m) = (3/2, 3/2)$  component. The weight of such band decreases monotonically for an increasing interdot distance, while that of the second largest contribution, namely  $(j, m) = (3/2, -1/2)$ , increases with increasing  $D$ ; the opposite behavior characterizes the state  $|\psi_3\rangle$ , belonging to the first excited Kramers doublet. In Table I we report the values of the band occupations corresponding to the smallest and largest values of  $a$  that we consider here. The occupation probabilities of the  $m = -3/2$  and of the  $j = 1/2$  subbands (not reported) for states  $|\psi_1\rangle$  and  $|\psi_3\rangle$  are negligible. The states  $|\psi_2\rangle$  and  $|\psi_4\rangle$  are the time-reversal conjugates of  $|\psi_1\rangle$  and  $|\psi_3\rangle$ , respectively. Therefore,  $p_{2,j,m} = p_{1,j,-m}$  and  $p_{4,j,m} = p_{3,j,-m}$ .

For different orientations of the small magnetic field, one obtains different occupations of the individual bands: for example, for  $\mathbf{B}$  along the  $x$  direction one has  $p_{1,j,m} = p_{1,j,-m}$ . This is due to the fact that the magnetic field,

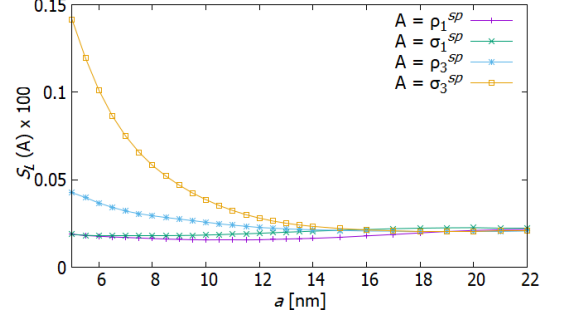


FIG. 3. Linear entropies (multiplied by a factor 100) of the reduced spin states  $\rho_\alpha^{\text{sp}}$  and of their dephased counterparts  $\sigma_\alpha^{\text{sp}}$  for the hole eigenstates  $|\psi_\alpha\rangle$  ( $\alpha = 1, 3$ ) of the Si double dot, as functions of the half interdot distance  $a$ . The maximum possible value for  $S_L(\rho_\alpha^{\text{sp}})$  is  $5/6 \approx 0.833$ .

in the weak-field regime that we are considering, selects different linear combinations of the degenerate Kramers states, depending on its orientation. However, the total occupation of the heavy- and light-hole bands for each Kramers doublet is independent of the field orientation.

The expectation values of the mirror symmetry operator  $\sigma_{yz}$  show that, in the considered range of parameter values, one can label the ground and first excited molecular spin-orbitals as spatially symmetric and antisymmetric states to a good degree of approximation. The band-resolved expectation values show that the symmetry along the  $x$  direction is well defined and coincides for the subbands  $(j, m)$  having the largest occupations, namely  $b = (3/2, 3/2)$  and  $b = (3/2, -1/2)$  (while it is undefined for the remaining ones). In fact, we find that in these cases  $|\langle\psi_{\alpha,b}|\sigma_{yz}|\psi_{\alpha,b}\rangle| > 0.99 \langle\psi_{\alpha,b}|\psi_{\alpha,b}\rangle$  in the whole considered range of values of  $a$ . The same inequality applies to the mirror symmetries about the two other coordinate planes.

We finally analyze the degree of entanglement between the spin and orbital degrees of freedom. In the case of Si (Fig. 3), the ground state displays a low degree of mixing between the subbands [low  $S_L(\sigma_1^{\text{sp}})$ ], which also implies a small degree of entanglement between spin and orbital components [low  $S_L(\rho_1^{\text{sp}})$ ]. In the case of the first excited state, the difference between the two entropies is significant, especially for the smallest values of the interdot distance. This corresponds to a significant amount of band mixing, where, however, the orbital components corresponding to the two main subbands,  $b = (3/2, 3/2)$  and  $b' = (3/2, -1/2)$ , have a large overlap. In fact, the normalized overlap  $|\langle\psi_{3,b}|\psi_{3,b'}\rangle|(p_{3,b}p_{3,b'})^{-1/2}$  decreases monotonically from 0.88 for  $a = 5$  nm to less than 0.01 for  $a = 22$  nm. In any case, as the interdot distance varies, we either find a small amount of band mixing, or a large overlap between the orbitals corresponding to the main spin components. Therefore, a well-defined spin state can be assigned to each of the hole eigenstates.

In the case of Ge, the eigenstates  $|\psi_\alpha\rangle$  (with  $\alpha = 1, 2, 3, 4$ ) display symmetry properties similar to those

of Si. However, the degree of band mixing is very limited, as the weight of the heavy-hole bands is higher than 0.999 and 0.997 respectively for the ground ( $\alpha = 1, 2$ ) and first excited states ( $\alpha = 3, 4$ ) in the whole investigated range of interdot distance values. Therefore, the linear entropies of both  $\rho_\alpha^{\text{sp}}$  and  $\sigma_\alpha^{\text{sp}}$  deviate negligibly from 0.

### III. TWO-HOLE STATES

From our numerical calculations performed with the full 6-band structure of the hole valence bands, we find that the occupation probability of the split-off bands ( $j = 1/2$ ) in the lowest-energy single-hole states is negligible, for the confinement potentials that we have considered. However, the split-off bands indirectly affect the overall band mixing, for they provide a coupling path between the light- and heavy-hole bands. Instead, the effect of these bands on the two-hole states is negligible. Therefore, in order to simplify the following discussion, we project the single-hole states onto the  $j = 3/2$  subspace before proceeding with the calculation of the two-hole states. As a consequence, all holes considered in the following have  $j = 3/2$ , and their individual spin state will be specified by the quantum number  $m$  only.

#### A. Method

##### 1. Diagonalization of the two-hole Hamiltonian

In the case of two spin-1/2 fermions (such as electrons in one band with  $l = 0$ ), one can combine the Slater determinants corresponding to different spin-orbitals in order to obtain a basis set formed by states with defined values of the total spin  $J = S \in \{0, 1\}$ . Each two-fermion state is the product either of a symmetric orbital and an antisymmetric spinor ( $J = 0$ ), or of an antisymmetric orbital and a symmetric spinor ( $J = 1$ ). The eigenstates of the Hamiltonian retain these symmetries.

In the case of spin-3/2 fermions, such as heavy and light holes in Si and Ge, it is still possible to combine the Slater determinants and obtain basis states that have a defined symmetry for both spin and orbital parts. In fact, one can introduce spinors  $|J, M\rangle$ , where  $J \in \{0, 1, 2, 3\}$  corresponds to the total spin and  $M = m_1 + m_2$  is the eigenvalue of the two-hole spin-projection operator  $J_z = j_{1,z} + j_{2,z}$ . States  $|J, M\rangle$  are either symmetric or antisymmetric with respect to particle exchange, depending on whether  $J$  is even or odd. Therefore, an odd- $J$  spinor must be combined with an antisymmetric orbital, and an even- $J$  spinor must be combined with a symmetric orbital, so that the product is antisymmetric. As a further complication with respect to the two-electron case, the hole Hamiltonian induces a mixing between symmetric and antisymmetric spinors, such that neither  $J$  nor its parity are good quantum numbers (see below).

The basis set for the two-hole states is constructed from a set of orthonormal single-hole states  $|\psi_\alpha\rangle$  [Eq. 12]. From these, one can define the two-hole Slater determinants

$$\begin{aligned} |\Phi_{\alpha\beta}\rangle &= \frac{1}{\sqrt{2}} (|\psi_\alpha\rangle|\psi_\beta\rangle - |\psi_\beta\rangle|\psi_\alpha\rangle) \\ &= \sum_{\zeta=\pm 1} \sum_{m_1 \geq m_2} |\Xi_{m_1, m_2}^{\alpha\beta\zeta}\rangle |\Upsilon_{m_1, m_2}^\zeta\rangle, \end{aligned} \quad (23)$$

where

$$|\Upsilon_{m_1 > m_2}^\zeta\rangle \equiv \frac{1}{\sqrt{2}} (|m_1\rangle|m_2\rangle - \zeta|m_2\rangle|m_1\rangle), \quad (24)$$

$$|\Upsilon_{m_1 = m_2}^\zeta\rangle \equiv \frac{1}{2}(1 - \zeta)|m_1\rangle|m_2\rangle \quad (25)$$

are the symmetric ( $\zeta = -1$ ) and antisymmetric ( $\zeta = +1$ ) combinations of the spinors  $|m_1\rangle|m_2\rangle$  and  $|m_2\rangle|m_1\rangle$ . In the  $j = 1/2$  case (electrons), such combinations coincide respectively with the triplet and singlet states. In the present  $j = 3/2$  case, the states  $|\Upsilon_{m_1 > m_2}^{-1}\rangle$  and  $|\Upsilon_{m_1 > m_2}^1\rangle$  belong respectively to the subspaces  $J \in \{1, 3\}$  and  $J \in \{0, 2\}$ , but each of them generally includes components from different  $J$  multiplets with the same parity.

In order to guarantee the overall symmetry of the two-hole state, the orbitals corresponding to the  $J \in \{0, 2\}$  and  $J \in \{1, 3\}$  subspaces must be symmetric and antisymmetric, respectively:

$$\begin{aligned} |\Xi_{m_1 > m_2}^{\alpha\beta\zeta}\rangle &\equiv \frac{1}{2} [|\psi_{\alpha, m_1}\rangle|\psi_{\beta, m_2}\rangle + \zeta|\psi_{\beta, m_2}\rangle|\psi_{\alpha, m_1}\rangle \\ &\quad - \zeta|\psi_{\alpha, m_2}\rangle|\psi_{\beta, m_1}\rangle - |\psi_{\beta, m_1}\rangle|\psi_{\alpha, m_2}\rangle], \\ |\Xi_{m_1 = m_2}^{\alpha\beta\zeta}\rangle &\equiv \frac{1 - \zeta}{2\sqrt{2}} [|\psi_{\alpha, m_1}\rangle|\psi_{\beta, m_2}\rangle - |\psi_{\beta, m_2}\rangle|\psi_{\alpha, m_1}\rangle]. \end{aligned} \quad (26)$$

The normalized states  $|\Upsilon_{m_1, m_2}^\zeta\rangle$  defined in spin space are mutually orthogonal. The orbitals  $|\Xi_{m_1, m_2}^{\alpha\beta\zeta}\rangle$  defined in real space, instead, are in general not normalized and not mutually orthogonal.

The two-hole eigenstates are obtained by means of a configuration-interaction approach. The first step is the diagonalization of the single-hole LK Hamiltonian, which gives the eigenstates  $|\psi_\alpha\rangle$  [Eq. 12], and the corresponding single-particle eigenvalues  $e_\alpha$ . From these, one constructs the basis for two-hole states, formed by the Slater determinants  $|\Phi_{\alpha\beta}\rangle$  [Eq. (23)]. In this basis, the total Hamiltonian is given by:

$$\begin{aligned} \langle \Phi_{\alpha\beta} | H | \Phi_{\alpha'\beta'} \rangle &= (e_\alpha + e_\beta) (\delta_{\alpha, \alpha'} \delta_{\beta, \beta'} - \delta_{\alpha, \beta'} \delta_{\beta, \alpha'}) \\ &\quad + V_C(\alpha\beta, \alpha'\beta'), \end{aligned} \quad (27)$$

where the Coulomb term reads as

$$\begin{aligned} V_C(\alpha\beta, \alpha'\beta') &= \sum_{m_1, m_2} \int d\mathbf{r}_1 d\mathbf{r}_2 \psi_{\alpha, m_1}^*(\mathbf{r}_1) \psi_{\beta, m_2}^*(\mathbf{r}_2) \\ &\quad \times V_C(\mathbf{r}_1 - \mathbf{r}_2) [\psi_{\alpha', m_1}(\mathbf{r}_1) \psi_{\beta', m_2}(\mathbf{r}_2) \\ &\quad - \psi_{\beta', m_1}(\mathbf{r}_1) \psi_{\alpha', m_2}(\mathbf{r}_2)], \end{aligned} \quad (28)$$

and  $\psi_{\alpha,m}(\mathbf{r}) = \langle \mathbf{r} | \psi_{\alpha,m} \rangle$ . We assume here a uniform screening,  $V_C(\mathbf{r}_1 - \mathbf{r}_2) = (\epsilon |\mathbf{r}_1 - \mathbf{r}_2|)^{-1}$ , quantified by the dielectric constants  $\epsilon_{\text{Si}} = 11.68$  for silicon and  $\epsilon_{\text{Ge}} = 16.2$  for germanium. As we have shown in Ref. 38, the Coulomb interaction also includes short-ranged inter-band processes, which can play a role in strongly confined systems. However, Eq. (28) is correct under the widely used approximation that the Coulomb potential is intraband.

The diagonalization of this matrix yields the two-hole eigenstates as linear combinations of the basis Slater determinants,

$$|\Psi_k\rangle \equiv \sum_{\alpha,\beta} C_{\alpha\beta}^k |\Phi_{\alpha\beta}\rangle \equiv \sum_{\zeta=\pm 1} \sum_{m_1 \geq m_2} |\Pi_{m_1,m_2}^{k\zeta}\rangle |\Upsilon_{m_1,m_2}^\zeta\rangle, \quad (29)$$

where

$$|\Pi_{m_1,m_2}^{k\zeta}\rangle \equiv \sum_{\alpha,\beta} C_{\alpha\beta}^k |\Xi_{m_1,m_2}^{\alpha\beta\zeta}\rangle, \quad (30)$$

and the coefficients  $C_{\alpha\beta}^k$ , which define the  $k$ -th eigenstate, result from the diagonalization of the two-hole Hamiltonian.

## 2. Characterization of the two-hole states

Analogously to the single-hole case, we define the spin reduced density matrix for the two-hole states:

$$\rho_k^{\text{tp}} \equiv \sum_{\zeta=\pm 1} \sum_{\substack{m_1 \geq m_2 \\ m'_1 \geq m'_2}} \langle \Pi_{m'_1,m'_2}^{k\zeta} | \Pi_{m_1,m_2}^{k\zeta} \rangle |\Upsilon_{m_1,m_2}^\zeta\rangle \langle \Upsilon_{m'_1,m'_2}^\zeta|. \quad (31)$$

From the reduced density matrix one can derive the weights of the  $J$  multiplets, which are given by:

$$p_{k,J} = \sum_{M=-J}^J p_{k,J,M} = \sum_{M=-J}^J \langle J, M | \rho_k^{\text{tp}} | J, M \rangle. \quad (32)$$

Since the length of the constituent spins is  $j = 3/2$ , the possible values of  $J$  range from 0 to 3.

The entanglement between spin and orbital components of the  $k$ -th two-hole eigenstate is quantified by the linear entropy

$$S_L(\rho_k^{\text{tp}}) = 1 - \text{tr}[(\rho_k^{\text{tp}})^2]. \quad (33)$$

Analogously to the case of single-hole states, here spin-orbit entanglement requires the distribution of the reduced spin states among different two-hole spinors ( $J, M$ ). However, for a given occupation of these spinors, the amount of entanglement (and thus the linear entropy of  $\rho_k^{\text{tp}}$ ) depends on the overlap between the corresponding orbital states. In order to single out the contributions

Si	$S(k=1)$		$T_0(k=3)$	
$a$ [nm]	5	14	5	14
$p_{k,0,0}$	0.490	0.487	0.000	0.000
$p_{k,2,0}$	0.477	0.488	0.000	0.006
$p_{k,2,\pm 2}$	0.012	0.001	0.008	0.012
$p_{k,1,0}$	0.000	0.000	0.860	0.878
$p_{k,3,0}$	0.000	0.000	0.099	0.098
$p_{k,3,\pm 2}$	0.004	0.005	0.012	0.005

Ge	$S(k=1)$		$T_0(k=3)$	
$a$ [nm]	12	34	12	34
$p_{k,0,0}$	0.499	0.499	0.000	0.000
$p_{k,2,0}$	0.499	0.499	0.000	0.000
$p_{k,2,\pm 2}$	0.000	0.000	0.000	0.000
$p_{k,1,0}$	0.000	0.000	0.897	0.898
$p_{k,3,0}$	0.000	0.000	0.100	0.100
$p_{k,3,\pm 2}$	0.000	0.000	0.000	0.000

TABLE II. Main occupation probabilities  $p_{k,J,M}$  corresponding to the  $k=1$  (singlet  $S$ ) and  $k=3$  (triplet  $T_0$ ) two-hole eigenstates and to the spin configuration ( $J, M$ ).

of these factors, we compare the linear entropy of the reduced spin state  $\rho_k^{\text{tp}}$  with that of its dephased counterpart

$$\sigma_k^{\text{tp}} = \sum_{\zeta=\pm 1} \sum_{m_1 \geq m_2} \langle \Pi_{m_1,m_2}^{k\zeta} | \Pi_{m_1,m_2}^{k\zeta} \rangle |\Upsilon_{m_1,m_2}^\zeta\rangle \langle \Upsilon_{m_1,m_2}^\zeta|. \quad (34)$$

The dephasing is performed in the  $(m_1, m_2)$  basis because the weights of the  $|\Upsilon_{m_1,m_2}^\zeta\rangle \langle \Upsilon_{m_1,m_2}^\zeta|$  projectors differ from one another, if the orbitals corresponding to different subbands are not parallel. One has that

$$S_L(\sigma_k^{\text{tp}}) \geq S_L(\rho_k^{\text{tp}}), \quad (35)$$

where the first entropy quantifies the mixing between the different  $(m_1, m_2)$  components, i.e., the spin-orbit entanglement that one would have if the orbitals corresponding to different bands were mutually orthogonal. The comparison between the above entropies thus allows one to estimate the degree of orthogonality between the orbitals corresponding to different values of  $(m_1, m_2)$ .

## B. Numerical results

We shall focus on the two lowest two-hole energy levels at zero magnetic field. The ground level is a singlet (state  $|S\rangle$ , corresponding in the following to  $k=1$ ), while the first excited level is a triplet of degenerate states ( $|T_- \rangle$ ,  $|T_0 \rangle$  and  $|T_+ \rangle$ , corresponding respectively to  $k=2, 3$  and 4). These degeneracies are analogous to those found in the single-band two-electron case. However, in that standard case singlet and triplet are eigenstates of  $\mathbf{J}^2$



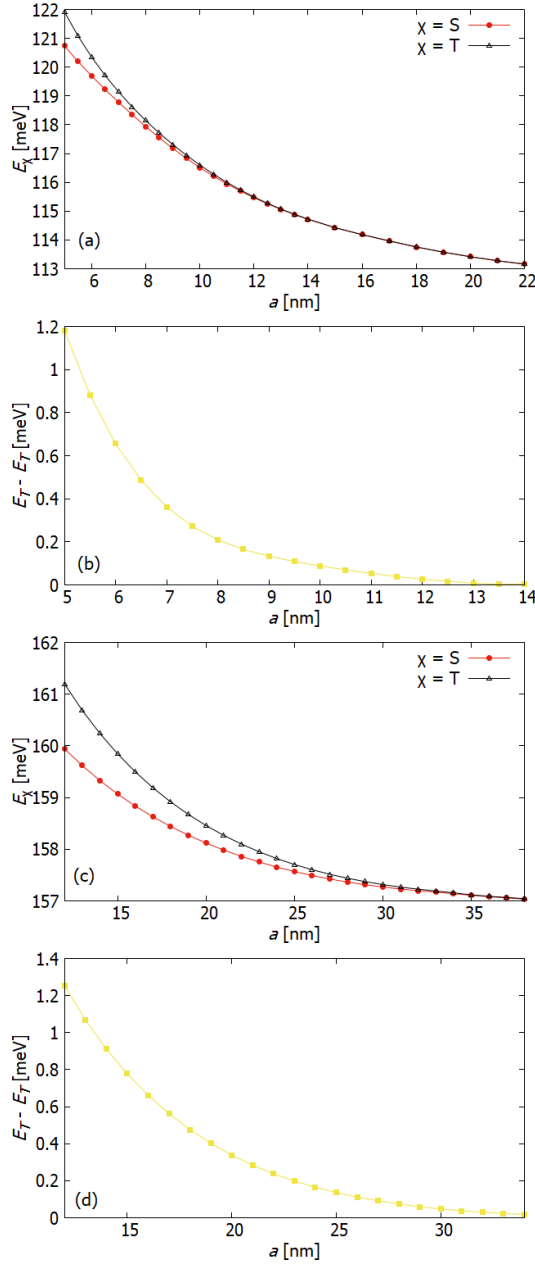


FIG. 4. Energy of the lowest singlet ( $E_S$ ), of the three degenerate first-excited states ( $E_T$ ) and singlet-triplet splitting ( $E_T - E_S$ ) as a function of the half interdot distance  $a$  for the cases of Si (a, b) and Ge (c, d). In panels (b, d) we report the kinetic and Coulomb (changed in sign) contributions to the singlet-triplet splitting.

with eigenvalues  $J = 0$  and  $J = 1$ , respectively, while the four-band two-hole case that we are treating is more complicated, as the eigenstates of the Hamiltonian are linear combinations of several two-particle spinors with different values of  $J$ .

The energy gap between the singlet and the triplet states decreases as a function of the interdot distance, faster than the tunneling-induced gap between the

single-particle bonding and antibonding states, for both Si and Ge quantum dots (Fig. 4). This is analogous to what is expected within a Hubbard-model picture, where the singlet-triplet energy splitting decays with the interdot distance as the second power of the hopping parameter.

We characterize the lowest two-hole eigenstates by means of the occupation probabilities  $p_{k,J,M}$  of the spinors  $(J, M)$  (Table II). This analysis shows that the dominant part of the singlet state has  $M = 0$  and is given by comparable contributions from  $J = 0$  and  $J = 2$  spinors, which are antisymmetric with respect to permutation of the spin components  $m_1$  and  $m_2$ . In the limit of vanishing band mixing, where the ground state has a purely heavy-hole character, the singlet state consists of a linear superposition of only these two contributions, with equal weights ( $p_{1,0,0} = p_{1,2,0} = \frac{1}{2}$ ). Here, the presence of a small light-hole component in the single-particle states produces two deviations from this ideal limit, namely: 1- the weights  $p_{1,0,0}$  and  $p_{1,2,0}$  slightly differ from one another, and minor contributions with  $(J, M) = (2, \pm 2)$  appear; 2- contributions from odd- $J$  (symmetric) spinors appear, as is seen from  $p_{1,3,\pm 2} \neq 0$ . Although the mixing between  $J$  subspaces with different symmetries is here very limited, it is allowed by the symmetries of the Hamiltonian, and always expected to some degree if the single-hole states are not factorized (see the discussion of this topic in Sections IV and V).

The triplet states are characterized by dominant contributions from  $J = 1$  and  $J = 3$  spinors, which have a symmetric character. In particular, the main terms of the  $T_0$  state have  $M = 0$ ; in the single (heavy-hole) band limit,  $p_{3,1,0} = \frac{9}{10}$  and  $p_{3,3,0} = \frac{1}{10}$ . The small light-hole component causes deviations from these limiting values, and the presence of additional contributions from the  $(J, M) = (3, \pm 2)$  states, as well as mixing with  $J = 2$  (antisymmetric) spinors. Finally, the  $T_{\pm}$  states are characterized by odd values of  $J$  and  $M$ , and tend to the maximally polarized states in the absence of a light-hole component ( $p_{2,3,-3} = p_{4,3,3} = 1$ ).

Overall, the dependence of the occupation probabilities  $p_{1,J,M}$  and  $p_{3,J,M}$  on the interdot distance is very weak, especially in the case of Ge. This is reflected in the dependence of the linear entropies on  $a$  (see Fig. 5 for the case of Si). For the reduced two-spin state  $\rho_k^{\text{tp}}$ , the linear entropy of both singlet and triplet is of the order of a few percents. One can thus associate well-defined spin states to the four lowest eigenstates. The entropy would vanish and one would reach the limit of purely spin states if the orbitals corresponding to the different spin states were parallel to each other. The opposite limit is the case where the orbitals corresponding to different bands are all mutually orthogonal. The reduced spin state would then coincide with the dephased spin state  $\sigma_k^{\text{tp}}$ , whose linear entropy is also plotted in Fig. 5 for a comparison. The difference between the linear entropy of  $\sigma_k^{\text{tp}}$  and that of  $\rho_k^{\text{tp}}$  thus represents an indicator of the orthogonality between the two-hole orbitals.

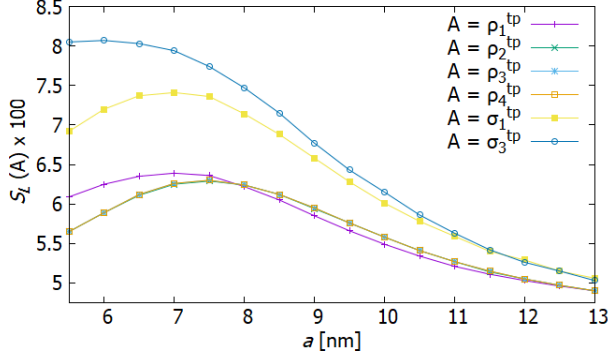


FIG. 5. Linear entropies (multiplied by a factor 100) of the reduced spin states  $\rho_k^{\text{tp}}$  and of their dephased counterparts  $\sigma_k^{\text{tp}}$  for the singlet and triplet states in the Si double dot. The maximum possible value of  $S_L(\rho_k^{\text{tp}})$  is  $15/16 = 0.9375$ .

#### IV. FOUR-BAND HUBBARD MODEL

We now build a semi-analytical Hubbard model that accounts for the main features of one- and two-hole DQD states in Si and Ge. The model reproduces with a good degree of approximation the numerical results presented in the previous Section, and - while including the complexity that originates from the four-band structure of the valence band - provides a more general and transparent physical picture.

In the spirit of the Hubbard model<sup>40</sup>, the DQD single- and two-hole states are derived from the single-hole eigenstates of the isolated dots. These correspond to the regions close to the minima of the confinement potential  $V(\mathbf{r})$ . For sufficiently large values of the interdot distance  $D = 2a$ , the single-dot orbitals centered in different dots are approximately orthogonal and form a convenient basis for the description of the DQD states. The simplest model is obtained by considering only the ground Kramers doublet for each of the two dots, for a total of four basis single-hole states. The complication of the present model, with respect to standard (one-band) Hubbard models, lies in the fact that we have to take into account the four-band structure of the basis states.

##### A. Derivation of the Hamiltonian

As a first step, we consider the single-hole Hamiltonian and divide the DQD potential in three parts, in order to isolate the single-dot contributions:

$$\hat{H}_{\text{DQD}} = \hat{H}_{\mathbf{k}\cdot\mathbf{p}} + \underbrace{\hat{V}_1 + \hat{V}_2 + \hat{V}_{12}}_{\hat{V}_{\text{DQD}}}. \quad (36)$$

Here,  $\hat{V}_s$ ,  $s \in \{1, 2\}$ , is the confining potential for dot  $s$  and  $\hat{V}_{12}$  is the “tunneling-enabling” potential (the difference between the total DQD potential and the sum of the separate dots’ potentials). The single-dot terms  $\hat{V}_s$  can

be identified with the potentials obtained by replacing, in  $V(\mathbf{r})$ , the double-dot expression  $V_{\text{DQD}}(x)$  with its harmonic approximation around either minimum [Eq. 11]. The definition of  $\hat{V}_s$  is not univocal, but the formulation of the model is independent on its exact expression, as long as the symmetry between the two dots is preserved.

The single-hole states that form the ground Kramers doublet within each of the two dots are given by

$$\begin{aligned} |\psi_{s,\uparrow}\rangle &= \sum_m |\psi_{s,\uparrow,m}\rangle \otimes |m\rangle, \\ |\psi_{s,\downarrow}\rangle &= \sum_m (-1)^{\frac{3}{2}-m} |\psi_{s,\uparrow,-m}^*\rangle \otimes |m\rangle, \end{aligned} \quad (37)$$

where  $m \in \{3/2, 1/2, -1/2, -3/2\}$  is the eigenvalue of  $j_z$ , and the relation between  $|\psi_{s,\uparrow}\rangle$  and  $|\psi_{s,\downarrow}\rangle$  results from time-reversal symmetry. The index  $\tau \in \{\uparrow, \downarrow\}$  specifies the eigenstate within the doublet and is akin, as we shall see, to the eigenvalue of the third component of a pseudospin-1/2 operator. The excited states of each single dot are assumed to lie at energies high enough that they can be neglected in the development of a low-energy model for the one- and two-hole states.

Numerical calculations performed on single-hole states of single dots suggest that, when  $\mathbf{B} = (B_x, 0, 0)$  and  $B_x \rightarrow 0$ , the orbitals satisfy

$$|\psi_{s,\uparrow,m}\rangle = |\psi_{s,\uparrow,-m}\rangle, \quad |\psi_{s,\downarrow,m}\rangle = -|\psi_{s,\downarrow,-m}\rangle \quad (38)$$

to a very good approximation; this constraint conveniently reduces the size of the functional space. Besides, the imaginary parts of the orbitals are negligible, compared to the real ones. In the following, we develop and solve the model assuming the validity of Eq. (38), and then discuss the simplifications introduced by the further assumption that the orbitals are real (end of Section IV B, and Section IV D). These approximations will be justified *a posteriori*, by comparing the results derived from the Hubbard model with those obtained from the full numerical approach (see Appendix A).

From Eq. (38), it follows that

$$\begin{aligned} |\psi_{s,\uparrow}\rangle &\equiv |\psi_{s,H}\rangle \otimes \left( \left| \frac{3}{2} \right\rangle + \left| -\frac{3}{2} \right\rangle \right) + |\psi_{s,L}\rangle \otimes \left( \left| \frac{1}{2} \right\rangle + \left| -\frac{1}{2} \right\rangle \right), \\ |\psi_{s,\downarrow}\rangle &\equiv |\psi_{s,H}^*\rangle \otimes \left( \left| \frac{3}{2} \right\rangle - \left| -\frac{3}{2} \right\rangle \right) - |\psi_{s,L}^*\rangle \otimes \left( \left| \frac{1}{2} \right\rangle - \left| -\frac{1}{2} \right\rangle \right), \end{aligned} \quad (39)$$

where  $|\psi_{s,H}\rangle \equiv |\psi_{s,\uparrow,\frac{3}{2}}\rangle$  and  $|\psi_{s,L}\rangle \equiv |\psi_{s,\uparrow,\frac{1}{2}}\rangle$  are the heavy- and light-hole orbitals for dot  $s$ .

If the interdot distance is large compared to the extension along  $x$  of the single-dot eigenstates  $|\psi_{s,\tau}\rangle$ , one has that:

$$\hat{V}_2 |\psi_{1,\tau}\rangle \approx 0, \quad \hat{V}_1 |\psi_{2,\tau}\rangle \approx 0, \quad \langle \psi_{1,\tau} | \psi_{2,\tau'} \rangle \approx 0, \quad (40)$$

while, by definition,

$$(\hat{H}_{\mathbf{k}\cdot\mathbf{p}} + \hat{V}_s) |\psi_{s,\tau}\rangle = E_{s,\tau} |\psi_{s,\tau}\rangle. \quad (41)$$

The matrix elements of the single-hole Hamiltonian are

$$\langle \psi_{s,\tau} | \hat{H}_{\text{DQD}} | \psi_{s',\tau'} \rangle = \delta_{\tau,\tau'} \left[ \delta_{s,s'} E_{s,\tau} + T_{s,s'}^{(\tau)} \right], \quad (42)$$

where

$$\begin{aligned} T_{s,s'}^{(\uparrow)} &= 2 \sum_{h \in \{H,L\}} \int d\mathbf{r} V_{12}(\mathbf{r}) \psi_{s,h}(\mathbf{r}) \psi_{s',h}(\mathbf{r}) \\ &= \langle \psi_{s,\uparrow} | \hat{V}_{12} | \psi_{s',\uparrow} \rangle = \langle \psi_{s,\downarrow} | \hat{V}_{12} | \psi_{s',\downarrow} \rangle^*, \\ T_{s,s'}^{(\downarrow)} &= \left[ T_{s,s'}^{(\uparrow)} \right]^*. \end{aligned} \quad (43)$$

In second quantization, the single-hole Hamiltonian resulting from the above considerations reads as

$$\hat{H}_{\text{DQD}} = \sum_{\tau} \sum_{s,s'} \left[ \delta_{s,s'} E_{s,\tau} + T_{s,s'}^{(\tau)} \right] \hat{\psi}_{s,\tau}^{\dagger} \hat{\psi}_{s',\tau}. \quad (44)$$

The on-site single-hole parameters ( $E_{1,\uparrow} = E_{2,\uparrow} = E_{1,\downarrow} = E_{2,\downarrow}$  and  $T_{1,1}^{(\uparrow)} = T_{2,2}^{(\uparrow)} = T_{1,1}^{(\downarrow)} = T_{2,2}^{(\downarrow)}$ ) only add a constant contribution to the eigenvalues, and can thus be neglected. The only relevant single-hole parameter is the one related to inter-site hopping:

$$T_{1,2}^{(\uparrow)} = \left[ T_{2,1}^{(\uparrow)} \right]^* = \left[ T_{1,2}^{(\downarrow)} \right]^* = T_{2,1}^{(\downarrow)} \equiv T. \quad (45)$$

In order to obtain an analytically solvable model, we assume that the interaction Hamiltonian is intraband and on-site. Its expression is thus given by

$$\hat{H}_U = \frac{1}{2} \sum_s \sum_{\tau_1, \tau_2, \tau_3, \tau_4} U_{\tau_1, \tau_2, \tau_3, \tau_4} \hat{\psi}_{s,\tau_1}^{\dagger} \hat{\psi}_{s,\tau_2}^{\dagger} \hat{\psi}_{s,\tau_3} \hat{\psi}_{s,\tau_4}, \quad (46)$$

where

$$\begin{aligned} U_{\tau_1, \tau_2, \tau_3, \tau_4} &= \sum_{m, m'} \int d\mathbf{r} \int d\mathbf{r}' \psi_{s,\tau_1,m}^*(\mathbf{r}) \psi_{s,\tau_2,m'}^*(\mathbf{r}') \\ &\quad \times V_{\text{Coulomb}}(\mathbf{r} - \mathbf{r}') \psi_{s,\tau_3,m}(\mathbf{r}) \psi_{s,\tau_4,m}(\mathbf{r}') \\ &\equiv \delta_{\tau_1, \tau_4} \delta_{\tau_2, \tau_3} U, \end{aligned} \quad (47)$$

and

$$\begin{aligned} U &\equiv 4 \int d\mathbf{r} \int d\mathbf{r}' \left\{ |\psi_{s,H}(\mathbf{r})|^2 + |\psi_{s,L}(\mathbf{r})|^2 \right\} \\ &\quad \times V_{\text{Coulomb}}(\mathbf{r} - \mathbf{r}') \left\{ |\psi_{s,H}(\mathbf{r}')|^2 + |\psi_{s,L}(\mathbf{r}')|^2 \right\}. \end{aligned} \quad (48)$$

The two-site Hubbard Hamiltonian resulting from the previous considerations is

$$\begin{aligned} \hat{H}_{\text{Hubbard}} &= \left[ T \left( \hat{\psi}_{1,\uparrow}^{\dagger} \hat{\psi}_{2,\uparrow} + \hat{\psi}_{2,\downarrow}^{\dagger} \hat{\psi}_{1,\downarrow} \right) + \text{h.c.} \right] \\ &\quad + U (\hat{n}_{1,\uparrow} \hat{n}_{1,\downarrow} + \hat{n}_{2,\uparrow} \hat{n}_{2,\downarrow}), \end{aligned} \quad (49)$$

where  $\hat{n}_{s,\tau} = \hat{\psi}_{s,\tau}^{\dagger} \hat{\psi}_{s,\tau}$ , and the hopping parameter  $T = |T|e^{i\theta}$  is, in general, complex.

The two-site Hubbard model can be solved analytically at any occupation number  $N \in \{0, 1, 2, 3, 4\}$ . We are interested here in the cases of  $N = 1$  and  $N = 2$ .

## B. Solution of the Hubbard model for one hole

In the case of  $N = 1$ , there are two energy eigenvalues, both doubly degenerate. The eigenvalues are  $e_{\pm} = \pm|T|$ , while the eigenstates

$$|\psi_{\pm,\tau}\rangle = \frac{1}{\sqrt{2}} \left( \hat{\psi}_{1,\tau}^{\dagger} \pm e^{-i\theta} \hat{\psi}_{2,\tau}^{\dagger} \right) |0\rangle, \quad (50)$$

are given by the expressions

$$\begin{aligned} |\psi_{\pm,\uparrow}\rangle &= \frac{1}{\sqrt{2}} \left[ (|\psi_{1,H}\rangle \pm e^{-i\theta} |\psi_{2,H}\rangle) \otimes (|\tfrac{3}{2}\rangle + |-\tfrac{3}{2}\rangle) \right. \\ &\quad \left. + (|\psi_{1,L}\rangle \pm e^{-i\theta} |\psi_{2,L}\rangle) \otimes (|\tfrac{1}{2}\rangle + |-\tfrac{1}{2}\rangle) \right], \\ |\psi_{\pm,\downarrow}\rangle &= \frac{1}{\sqrt{2}} \left[ (|\psi_{1,H}^*\rangle \pm e^{-i\theta} |\psi_{2,H}^*\rangle) \otimes (|\tfrac{3}{2}\rangle - |-\tfrac{3}{2}\rangle) \right. \\ &\quad \left. - (|\psi_{1,L}^*\rangle \pm e^{-i\theta} |\psi_{2,L}^*\rangle) \otimes (|\tfrac{1}{2}\rangle - |-\tfrac{1}{2}\rangle) \right]. \end{aligned} \quad (51)$$

Under the (numerically justified) approximation that the single-dot orbitals are real, the hopping parameter  $T$  is real as well. In this case, see from Eqs. (51) that, despite the complexity associated with the four-band single-hole Hamiltonian, the single-hole eigenstates of the Hubbard model retain the bonding or anti-bonding character of the orbital wave functions that characterizes the single-band cases. This is consistent with our numerical results in the regime of weak coupling between the dots, as discussed in Subsec. II B. According to Eqs. (51), the sign of  $T$  (i.e., whether  $e^{-i\theta} = -1$  or  $+1$ ) determines the ordering of the single-hole eigenstates; our numerical results are consistent with  $T < 0$  (i.e.,  $e^{-i\theta} = -1$ ), yielding a bonding ground state, as in natural diatomic molecules. We mention that in different 4-band systems, such as vertically coupled DQDs in InGaAs/GaAs, also the alternative possibility of having  $T > 0$  and an anti-bonding ground state has been reported<sup>2,34,35</sup>.

## C. Solution of the Hubbard model for two holes

In the case of  $N = 2$ , there are six eigenstates and four distinct energy levels (three singlets and one triplet). It is convenient to write the basis states as

$$\begin{aligned} |\mathbb{S}\rangle &\equiv \frac{1}{\sqrt{2}} \left( \hat{\psi}_{1,\uparrow}^{\dagger} \hat{\psi}_{2,\downarrow}^{\dagger} - \hat{\psi}_{1,\downarrow}^{\dagger} \hat{\psi}_{2,\uparrow}^{\dagger} \right) |0\rangle, \\ |\mathbb{T}_{\uparrow}\rangle &\equiv \hat{\psi}_{1,\uparrow}^{\dagger} \hat{\psi}_{2,\uparrow}^{\dagger} |0\rangle, \\ |\mathbb{T}_0\rangle &\equiv \frac{1}{\sqrt{2}} \left( \hat{\psi}_{1,\uparrow}^{\dagger} \hat{\psi}_{2,\downarrow}^{\dagger} + \hat{\psi}_{1,\downarrow}^{\dagger} \hat{\psi}_{2,\uparrow}^{\dagger} \right) |0\rangle, \\ |\mathbb{T}_{\downarrow}\rangle &\equiv \hat{\psi}_{1,\downarrow}^{\dagger} \hat{\psi}_{2,\downarrow}^{\dagger} |0\rangle, \\ |\mathbb{D}_{-}\rangle &\equiv \frac{1}{\sqrt{2}} \left( \hat{\psi}_{1,\uparrow}^{\dagger} \hat{\psi}_{1,\downarrow}^{\dagger} - \hat{\psi}_{2,\uparrow}^{\dagger} \hat{\psi}_{2,\downarrow}^{\dagger} \right) |0\rangle, \\ |\mathbb{D}_{+}\rangle &\equiv \frac{1}{\sqrt{2}} \left( \hat{\psi}_{1,\uparrow}^{\dagger} \hat{\psi}_{1,\downarrow}^{\dagger} + \hat{\psi}_{2,\uparrow}^{\dagger} \hat{\psi}_{2,\downarrow}^{\dagger} \right) |0\rangle. \end{aligned} \quad (52)$$

From the diagonalization of the Hubbard Hamiltonian for  $N = 2$ , we obtain the following results. In terms of the exchange energy

$$J \equiv \frac{\sqrt{U^2 + 16|T|^2} - U}{2}, \quad (53)$$

the lowest energy level is  $E = -J$  and it corresponds to the eigenstate

$$|-J\rangle = \frac{2|T| \left[ -\cos(\theta)|\mathbb{S}\rangle - i\sin(\theta)|\mathbb{T}_0\rangle \right] - E_-|\mathbb{D}_+\rangle}{\sqrt{4|T|^2 + (E_-)^2}}. \quad (54)$$

The energy level  $E = 0$  corresponds to the following three degenerate eigenstates:

$$\begin{aligned} |T_{x,0}\rangle &= -\cos(\theta)|\mathbb{T}_0\rangle - i\sin(\theta)|\mathbb{S}\rangle \\ |T_{x,+}\rangle &= |\mathbb{T}_\uparrow\rangle, \quad |T_{x,-}\rangle = |\mathbb{T}_\downarrow\rangle. \end{aligned} \quad (55)$$

The energy level  $E = U$  corresponds to the eigenstate

$$|U\rangle = |\mathbb{D}_-\rangle, \quad (56)$$

the eigenvalue  $E = U + J$  corresponds to the eigenstate

$$|U + J\rangle = \frac{2|T| \left[ -\cos(\theta)|\mathbb{S}\rangle - i\sin(\theta)|\mathbb{T}_0\rangle \right] - E_+|\mathbb{D}_+\rangle}{\sqrt{4|T|^2 + (E_+)^2}}. \quad (57)$$

It should be noticed that, in the case of a real hopping parameter ( $\theta \in \{0, \pi\}$ ), the  $|\mathbb{T}_0\rangle$  components in the singlets vanish, just like the  $|\mathbb{S}\rangle$  component in the triplet. One thus recovers the formal results of the standard Hubbard model.

#### D. Spin-orbital wave functions for the low-energy two-hole eigenstates

In order to gain a deeper physical understanding of the two-hole eigenstates, we determine the corresponding spin-orbital wave functions. By combining Eqs. (39) and (52), one can write the expressions for the two-hole eigenstates of the Hubbard model explicitly. The resulting expressions are unwieldy in the most general case, but can be simplified by assuming that the orbital wave functions are real, as we already did in the case of  $N = 1$  (see the end of Section IV B). In the limit of  $|T| \ll U$ , one can neglect the double-occupancy states contributing to the ground state, and

$$|-J\rangle \approx |\mathbb{S}\rangle. \quad (58)$$

The lowest singlet and triplet states thus coincide with the (single-occupancy) eigenstates of an effective pseudospin-1/2 Heisenberg Hamiltonian,

$$\hat{H}_{\text{Heisenberg}} = J \left( \hat{\mathbf{S}}_1 \cdot \hat{\mathbf{S}}_2 - \frac{1}{4} \right), \quad (59)$$

where

$$\hat{\mathbf{S}}_s = \frac{1}{2} \sum_{\tau, \tau' \in \{\uparrow, \downarrow\}} \hat{\psi}_{s,\tau}^\dagger \boldsymbol{\sigma}_{\tau, \tau'} \hat{\psi}_{s,\tau'}, \quad (60)$$

is the pseudospin operator for site  $s \in \{1, 2\}$ , and  $\boldsymbol{\sigma}$  is the vector of Pauli matrices.

While the ground state is uniquely determined, the triplet states are degenerate, so we can consider any set of three orthogonal linear combinations of them. To facilitate the comparison with the numerical results (see Sections II B and III B, and Appendix A), we look for linear combinations of the triplet states that are compatible with those found numerically at  $\mathbf{B} = (0, 0, B_z)$ ,  $B_z \rightarrow 0$ . We find that, under the assumption that the wave functions are real, the sought-after combinations are

$$\begin{aligned} |T_{z,0}\rangle &\equiv \frac{1}{\sqrt{2}}|\mathbb{T}_\uparrow\rangle - \frac{1}{\sqrt{2}}|\mathbb{T}_\downarrow\rangle, \\ |T_{z,+}\rangle &\equiv \frac{1}{2}|\mathbb{T}_\uparrow\rangle + \frac{1}{\sqrt{2}}|\mathbb{T}_0\rangle + \frac{1}{2}|\mathbb{T}_\downarrow\rangle, \\ |T_{z,-}\rangle &\equiv \frac{1}{2}|\mathbb{T}_\uparrow\rangle - \frac{1}{\sqrt{2}}|\mathbb{T}_0\rangle + \frac{1}{2}|\mathbb{T}_\downarrow\rangle. \end{aligned} \quad (61)$$

We switch from the spinor basis  $|m_1, m_2\rangle$  to the spinor basis  $|J, M\rangle$ , where  $M = m_1 + m_2$  and  $J \in \{0, 1, 2, 3\}$ . The change of basis is achieved through the Clebsch-Gordan transformation, see Table III. We also introduce the condensed notation

$$\begin{aligned} |\Psi_{sh,s'h'}^S\rangle &\equiv |\psi_{sh}\rangle|\psi_{s'h'}\rangle + |\psi_{s'h'}\rangle|\psi_{sh}\rangle, \\ |\Psi_{sh,s'h'}^A\rangle &\equiv |\psi_{sh}\rangle|\psi_{s'h'}\rangle - |\psi_{s'h'}\rangle|\psi_{sh}\rangle, \end{aligned} \quad (62)$$

which identifies symmetric and anti-symmetric two-hole orbitals; here  $h, h' \in \{H, L\}$  denote the hole types.

We now list the resulting spin-orbital wave functions. The singlet ground state is

$$\begin{aligned} |\mathbb{S}\rangle &= \left( |\Psi_{1H,2H}^S\rangle + |\Psi_{1L,2L}^S\rangle \right) \otimes |0, 0\rangle \\ &+ \left( |\Psi_{1H,2H}^S\rangle - |\Psi_{1L,2L}^S\rangle \right) \otimes |2, 0\rangle \\ &+ \frac{1}{\sqrt{2}} \left( |\Psi_{1L,2H}^S\rangle + |\Psi_{1H,2L}^S\rangle \right) \otimes \left( |2, 2\rangle + |2, -2\rangle \right) \\ &+ \frac{1}{\sqrt{2}} \left( |\Psi_{1L,2H}^A\rangle - |\Psi_{1H,2L}^A\rangle \right) \otimes \left( |3, 2\rangle - |3, -2\rangle \right), \end{aligned} \quad (63)$$

and the triplet states are

$$\begin{aligned} |T_{z,+}\rangle &= \sqrt{2}|\Psi_{1H,2H}^A\rangle \otimes |3, 3\rangle \\ &+ \sqrt{2}|\Psi_{1L,2L}^A\rangle \otimes \left( \sqrt{\frac{2}{5}}|1, -1\rangle + \sqrt{\frac{3}{5}}|3, -1\rangle \right) \\ &+ \left( |\Psi_{1L,2H}^A\rangle + |\Psi_{1H,2L}^A\rangle \right) \otimes \left( \sqrt{\frac{3}{5}}|1, 1\rangle \right. \\ &\quad \left. - \sqrt{\frac{2}{5}}|3, 1\rangle \right) + \left( |\Psi_{1L,2H}^S\rangle - |\Psi_{1H,2L}^S\rangle \right) \otimes |2, 1\rangle, \end{aligned} \quad (64)$$

$ J, M\rangle$	$S_{3/2, M-3/2}^J$	$S_{1/2, M-1/2}^J$	$S_{-1/2, M+1/2}^J$	$S_{-3/2, M+3/2}^J$
$ 0, 0\rangle$	$-1/2$	$1/2$	$-1/2$	$1/2$
$ 1, 1\rangle$	$\sqrt{3}/\sqrt{10}$	$-2/\sqrt{10}$	$\sqrt{3}/\sqrt{10}$	$-$
$ 1, 0\rangle$	$3/\sqrt{20}$	$-1/\sqrt{20}$	$-1/\sqrt{20}$	$3/\sqrt{20}$
$ 1, -1\rangle$	$-$	$-\sqrt{3}/\sqrt{10}$	$2/\sqrt{10}$	$-\sqrt{3}/\sqrt{10}$
$ 2, 2\rangle$	$-1/\sqrt{2}$	$1/\sqrt{2}$	$-$	$-$
$ 2, 1\rangle$	$-1/\sqrt{2}$	$-$	$1/\sqrt{2}$	$-$
$ 2, 0\rangle$	$-1/2$	$-1/2$	$1/2$	$1/2$
$ 2, -1\rangle$	$-$	$1/\sqrt{2}$	$-$	$-1/\sqrt{2}$
$ 2, -2\rangle$	$-$	$-$	$-1/\sqrt{2}$	$1/\sqrt{2}$
$ 3, 3\rangle$	$1$	$-$	$-$	$-$
$ 3, 2\rangle$	$1/\sqrt{2}$	$1/\sqrt{2}$	$-$	$-$
$ 3, 1\rangle$	$-1/\sqrt{5}$	$-\sqrt{3}/\sqrt{5}$	$-1/\sqrt{5}$	$-$
$ 3, 0\rangle$	$1/\sqrt{20}$	$3/\sqrt{20}$	$3/\sqrt{20}$	$1/\sqrt{20}$
$ 3, -1\rangle$	$-$	$1/\sqrt{5}$	$\sqrt{3}/\sqrt{5}$	$1/\sqrt{5}$
$ 3, -2\rangle$	$-$	$-$	$1/\sqrt{2}$	$1/\sqrt{2}$
$ 3, -3\rangle$	$-$	$-$	$-$	$1$

TABLE III. Clebsch–Gordan coefficients  $S_{m_1, M-m_1}^J$  that define the decomposition of the states  $|J, M\rangle$  in terms of the states  $|m_1, m_2\rangle$ , for  $j_1 = j_2 = 3/2$ . Specifically,  $|J, M\rangle = \sum_{m_1} S_{m_1, M-m_1}^J |m_1, M-m_1\rangle$ . We use the Condon–Shortley phase convention.

$$\begin{aligned}
|T_{z,0}\rangle &= \frac{1}{\sqrt{2}} \left( |\Psi_{1L,2H}^A\rangle + |\Psi_{1H,2L}^A\rangle \right) \otimes (|3, 2\rangle + |3, -2\rangle) \\
&+ \frac{1}{\sqrt{2}} \left( |\Psi_{1L,2H}^S\rangle - |\Psi_{1H,2L}^S\rangle \right) \otimes (|2, 2\rangle - |2, -2\rangle) \\
&+ \sqrt{\frac{1}{5}} \left[ (3|\Psi_{1H,2H}^A\rangle - |\Psi_{1L,2L}^A\rangle) \otimes |1, 0\rangle \right. \\
&\left. + (|\Psi_{1H,2H}^A\rangle + 3|\Psi_{1L,2L}^A\rangle) \otimes |3, 0\rangle \right], \quad (65)
\end{aligned}$$

and

$$\begin{aligned}
|T_{z,-}\rangle &= \sqrt{2} |\Psi_{1H,2H}^A\rangle \otimes |3, -3\rangle \\
&- \sqrt{2} |\Psi_{1L,2L}^A\rangle \otimes \left( \sqrt{\frac{2}{5}} |1, 1\rangle + \sqrt{\frac{3}{5}} |3, 1\rangle \right) \\
&- \left( |\Psi_{1L,2H}^A\rangle + |\Psi_{1H,2L}^A\rangle \right) \otimes \left( \sqrt{\frac{3}{5}} |1, -1\rangle \right. \\
&\left. - \sqrt{\frac{2}{5}} |3, -1\rangle \right) + \left( |\Psi_{1L,2H}^S\rangle - |\Psi_{1H,2L}^S\rangle \right) \otimes |2, -1\rangle. \quad (66)
\end{aligned}$$

The good agreement between this analytical theory and the numerical results is discussed in Appendix A.

One of the interesting features of the two-hole states is that they are not eigenstates of the total operators  $\hat{\mathbf{J}}^2$  and  $\hat{J}_z$ . Therefore, as seen from the expressions (63), (64), (65) and (66), they are linear combinations of two-hole spinors  $|J, M\rangle$ , with various values of  $J$  and  $M$ . Moreover, the spinors contributing to each state do not all have the same symmetry under exchange of the two

particles, and consequently the same holds true for the orbitals. Therefore, two-hole eigenstates cannot be factorized as products of orbital and spin parts. This mixing is a peculiar feature of the four-band system, which is strikingly different from more common one-band systems. However, we have found numerically that the weights of the antisymmetric orbitals in the singlet and of the symmetric orbitals in the triplet are small (details are given in Section III B and Appendix A). The smallness of these terms, in the systems that we have considered, can be interpreted as a consequence of the small degree of entanglement between orbital and spin degrees of freedom, which we have already demonstrated via the calculation of the linear entropies associated with the spin reduced density matrix. We discuss this connection in Section V.

We also notice that, within the present model, non-zero light-hole components are necessary for the even-odd  $J$  mixing: if we were to set  $|\psi_{sL}\rangle \rightarrow 0$ , the two-hole states would reduce to

$$\begin{aligned}
|S\rangle &\rightarrow \sqrt{2} |\Psi_{1H,2H}^S\rangle \otimes \frac{1}{\sqrt{2}} (|0, 0\rangle + |2, 0\rangle), \\
|T_{z,+}\rangle &\rightarrow \sqrt{2} |\Psi_{1H,2H}^A\rangle \otimes |3, 3\rangle, \\
|T_{z,0}\rangle &\rightarrow \sqrt{2} |\Psi_{1H,2H}^A\rangle \otimes \sqrt{\frac{1}{10}} (3|1, 0\rangle + |3, 0\rangle), \\
|T_{z,-}\rangle &\rightarrow \sqrt{2} |\Psi_{1H,2H}^A\rangle \otimes |3, -3\rangle. \quad (67)
\end{aligned}$$

These are in agreement with the single-band limits discussed in Section III B.

## V. PSEUDOSPIN REPRESENTATION OF THE ONE- AND TWO-HOLE STATES

In view of the limited amount of mixing between the orbital and spin components in the lowest single-hole eigenstates, one can approximately describe them in terms of spin states alone.

### A. Single-hole states

In particular, the single-hole states  $|\psi_\alpha\rangle$ , with  $\alpha = 1, 2, 3, 4$ , are here characterized by a dominant heavy-hole component  $m = \pm 3/2$  and a significant contribution from the light-hole  $m = \mp 1/2$  (see Table I in Subsec. II B). Besides, both single- and two-hole lowest-energy states display a limited amount of entanglement between the spin and orbital degrees of freedom. As a reference for the actual reduced spin states, we consider hereafter the limiting case where such entanglement is exactly zero, due to a perfect overlap between the orbital states corresponding to the different bands:

$$|\psi_{s,L}\rangle \approx -r|\psi_{s,H}\rangle, \quad |\psi_{s,H}\rangle \approx |\psi_{s,H}^*\rangle, \quad |\psi_{s,L}\rangle \approx |\psi_{s,L}^*\rangle, \quad (68)$$



with  $s \in \{1, 2\}$ . One has  $r^2 = p_{i,\mp 1/2}/p_{i,\pm 3/2}$ ; the particular case of  $r = 0$  reproduces the single-band limit [see Eqs. (67)]. The approximation (68), for arbitrary  $r$ , amounts to freezing the orbital degrees of freedom, since it implies that there is only one independent orbital function for each dot; the single-hole states are then factorized as in Eq. (15).

This allows us to introduce a pseudospin-1/2 representation for the single-hole states localized in each dot, and express them exclusively in terms of the eigenstates  $|m\rangle$  of  $j_z$ :

$$\begin{aligned} |\uparrow\rangle_s &\equiv \frac{1}{\sqrt{1+r^2}} \left( \left| \frac{3}{2} \right\rangle_s - r \left| -\frac{1}{2} \right\rangle_s \right), \\ |\downarrow\rangle_s &\equiv \frac{1}{\sqrt{1+r^2}} \left( \left| -\frac{3}{2} \right\rangle_s - r \left| \frac{1}{2} \right\rangle_s \right). \end{aligned} \quad (69)$$

Each spinor for site  $s$  incorporates the heavy-hole orbital wave function for dot  $s$ , namely,  $\psi_{s,H}(\mathbf{r})$ .

## B. Two-hole states

The four lowest two-holes states in the pseudospin-1/2 representation are obtained from Eqs. (63), (64), (65) and (66) by applying the approximations (68) to the single-hole orbitals that constitute the two-hole orbitals. Equivalently, the same states can be obtained by writing the singlet and triplet states for the two pseudospin-1/2 single hole states,

$$\begin{aligned} |S^{\text{ps}}\rangle &= \frac{1}{\sqrt{2}} (|\downarrow, \uparrow\rangle - |\uparrow, \downarrow\rangle), \\ |T_+^{\text{ps}}\rangle &= |\uparrow, \uparrow\rangle, \\ |T_0^{\text{ps}}\rangle &= \frac{1}{\sqrt{2}} (|\downarrow, \uparrow\rangle + |\uparrow, \downarrow\rangle), \\ |T_-^{\text{ps}}\rangle &= |\downarrow, \downarrow\rangle \end{aligned} \quad (70)$$

(where the first and second positions correspond to the spins localized in the first and second dots, respectively), and replacing the states  $|\uparrow\rangle$  and  $|\downarrow\rangle$  with the expressions given in Eqs. (69). One obtains

$$\begin{aligned} |S^{\text{ps}}\rangle &= \frac{1}{1+r^2} \left[ \frac{1}{\sqrt{2}} (1+r^2) |0, 0\rangle \right. \\ &\quad \left. + \frac{1}{\sqrt{2}} (1-r^2) |2, 0\rangle - r (|2, 2\rangle + |2, -2\rangle) \right], \end{aligned} \quad (71)$$

$$\begin{aligned} |T_+^{\text{ps}}\rangle &= \frac{1}{1+r^2} \left[ |3, 3\rangle + r^2 \left( \sqrt{\frac{2}{5}} |1, -1\rangle + \sqrt{\frac{3}{5}} |3, -1\rangle \right) \right. \\ &\quad \left. - \sqrt{2} r \left( \sqrt{\frac{3}{5}} |1, 1\rangle - \sqrt{\frac{2}{5}} |3, 1\rangle \right) \right], \end{aligned} \quad (72)$$

$$\begin{aligned} |T_0^{\text{ps}}\rangle &= \frac{1}{1+r^2} \left[ -r (|3, 2\rangle + |3, -2\rangle) \right. \\ &\quad \left. + \sqrt{\frac{1}{10}} (3-r^2) |1, 0\rangle + \sqrt{\frac{1}{10}} (1+3r^2) |3, 0\rangle \right], \end{aligned} \quad (73)$$

and

$$\begin{aligned} |T_-^{\text{ps}}\rangle &= \frac{1}{1+r^2} \left[ |3, -3\rangle - r^2 \left( \sqrt{\frac{2}{5}} |1, 1\rangle + \sqrt{\frac{3}{5}} |3, 1\rangle \right) \right. \\ &\quad \left. + \sqrt{2} r \left( \sqrt{\frac{3}{5}} |1, -1\rangle - \sqrt{\frac{2}{5}} |3, -1\rangle \right) \right]. \end{aligned} \quad (74)$$

It is intended that the two-hole spinors  $|J, M\rangle$  incorporate the information about the two-hole orbitals; namely, the spinors with even  $J$  (antisymmetric) incorporate  $\Psi_{1H,2H}^S(\mathbf{r}_1, \mathbf{r}_2)$ , while the spinors with odd  $J$  (symmetric) incorporate  $\Psi_{1H,2H}^A(\mathbf{r}_1, \mathbf{r}_2)$ .

By comparing the two-hole spinors entering Eqs. (71), (72), (73) and (74) with those entering the Hubbard states, we notice that the difference of antisymmetric orbitals that multiplies the  $J = 3$  spinors in the Hubbard singlet [Eq. (63)] cancels out after the approximation (68), just as the differences between symmetric orbitals multiplying the  $J = 2$  spinors in the triplet states [Eqs. (64), (65) and (66)]. The singlet now contains only spinors with even  $J$  (antisymmetric), while the triplet contains only spinors with odd  $J$  (symmetric); accordingly, the whole singlet has the symmetric orbital  $\Psi_{1H,2H}^S(\mathbf{r}_1, \mathbf{r}_2)$ , while the whole triplet has the antisymmetric orbital  $\Psi_{1H,2H}^A(\mathbf{r}_1, \mathbf{r}_2)$ .

Therefore, within the Hubbard model the source of even/odd mixing is the difference in the spatial dependence (non-parallelism) of the heavy-hole and light-hole orbitals, as we have just seen that, when this difference is removed, the mixing disappears. However, the two-hole states in the pseudospin-1/2 formalism are still not eigenstates of  $\hat{\mathbf{J}}^2$  and  $\hat{J}_z$ , an effect of spin-orbit coupling. At the single-hole level, this can be traced to the fact that it is not possible to choose a basis of single-hole states which are eigenstates of  $\hat{J}_z$  [see Eqs. (69)].

## VI. CONCLUSIONS

We have investigated the properties of single- and two-hole states in horizontally-coupled Si and Ge quantum dots. In particular, we propose the use of entanglement measures such as the linear entropy in order to quantify the band mixing at the single- and two-hole level. On the other hand, the entropy of suitably dephased spin states quantifies the mixing in the standard band basis. In the two-hole case, the spin states corresponding to the lowest-energy eigenstates display similarities and differences with respect to the singlet and triplet states that

one obtains in the two-electron (one-band) case. In particular, the singlet ground state and the triplet excited states are dominantly antisymmetric and symmetric with respect to spin exchange, respectively, as in the electron case. However, they display a strong and coherent  $J$ -mixing, even in the single-band limit. The presence of light-hole components results in  $M$ -mixing within spin subspaces of the same symmetry, as well as in small contributions from spin subspaces with opposite symmetry with respect to the dominant one. The numerical results, obtained for representative Si and Ge double-dot geometries, are supported by an analytic derivation of the spin states, performed within a generalized Hubbard model approach.

### ACKNOWLEDGMENTS

The authors acknowledge financial support from the European Commission through the project IQubits (Call: H2020-FETOPEN-2018-2019-2020-01, Project ID: 829005).

### Appendix A: Comparison between the Hubbard model and the numerical results

In order to compare the predictions of the Hubbard model with our numerical results, we consider the weights of the  $(J, M)$  components of the four lowest two-hole states, i.e.,  $p_{k,J,M}$ , with  $k \in \{1, 2, 3, 4\}$  corresponding to the states  $\{\mathbb{S}, T_{z,+}, T_{z,0}, T_{z,-}\}$ . From the expressions of the two-hole states, Eqs. (63), (64), (65), and (66), we see that the Hubbard model predicts precise relationships between the weights of certain  $(J, M)$  components in different states, or within the same state. These relationships, which hold independently of the specific form of the single-hole wave functions, are:

$$\begin{aligned} p_{1,2,2} &= p_{1,2,-2}, & p_{1,3,2} &= p_{1,3,-2}, \\ p_{2,3,3} &= p_{4,3,-3}, & p_{2,1,-1} &= p_{4,1,1}, & p_{2,3,-1} &= p_{4,3,1}, \\ p_{2,1,1} &= p_{4,1,-1}, & p_{2,3,1} &= p_{4,3,-1}, & p_{2,2,1} &= p_{4,2,-1}; \end{aligned} \quad (\text{A1})$$

$$\begin{aligned} p_{3,1,0} + p_{3,3,0} - p_{2,3,3} - \frac{5}{2}p_{2,1,-1} \\ = p_{3,1,0} + p_{3,3,0} - p_{4,3,-3} - \frac{5}{2}p_{4,1,1} = 0; \end{aligned} \quad (\text{A2})$$

$$\begin{aligned} \frac{p_{2,1,1}}{p_{2,3,1}} &= \frac{p_{2,3,-1}}{p_{2,1,-1}} = \frac{p_{4,1,-1}}{p_{4,3,-1}} = \frac{p_{4,3,1}}{p_{4,1,1}} = \frac{3}{2}, \\ \frac{p_{2,3,1}}{p_{3,3,2}} &= \frac{p_{4,3,-1}}{p_{3,3,2}} = \frac{4}{5}, \\ \frac{p_{2,2,1}}{p_{3,2,2}} &= \frac{p_{4,2,-1}}{p_{3,2,2}} = 2. \end{aligned} \quad (\text{A3})$$

quantity	model	$a = 5$ nm	$a = 10$ nm	$a = 14$ nm
$p_{2,1,1}/p_{2,3,1}$	1.5	1.515	1.500	1.500
$p_{4,1,-1}/p_{4,3,-1}$	1.5	1.488	1.500	1.500
$p_{2,3,1}/p_{3,3,2}$	0.8	0.795	0.800	0.809
$p_{4,3,-1}/p_{3,3,2}$	0.8	0.803	0.800	0.809
$p_{2,2,1}/p_{3,2,2}$	2	1.987	2.000	2.000
$p_{4,2,-1}/p_{3,2,2}$	2	1.987	2.000	2.000

TABLE IV. Comparison between the predictions of the Hubbard model and the numerical results.

Moreover, the model predicts certain quantities  $p_{k,J,M}$  to be zero, since each of the states  $\{\mathbb{S}, T_{z,+}, T_{z,0}, T_{z,-}\}$  only involves 6 spinors  $|J, M\rangle$  out of 16.

To estimate the accuracy of the model, we compare its predictions with the two-hole calculations performed for silicon, in the exemplary cases of  $a \in \{5, 10, 14\}$  nm. The results of the comparison apply similarly to all the other calculations that we have performed, for both silicon and germanium.

We find that all the identities (A1) and the linear combinations (A2) are satisfied within an error  $\lesssim 10^{-4}$ , which is comparable to the estimated accuracy of the numerical calculations. The ratios given by Eqs. (A3) are shown in Table IV: the second column provides the model prediction, while columns 3–5 provide the numerical results for the three cases that we are considering. Some of the weights ( $p_{2,3,-1}$ ,  $p_{2,1,-1}$ ,  $p_{4,3,1}$  and  $p_{4,1,1}$ ) involved in Eqs. (A3) are found to be  $\approx 10^{-4}$ , which is below the estimated accuracy of the numerical calculations; therefore, computing their ratios is not significant, and we omit those from our analysis. This smallness can be interpreted within the Hubbard model by assuming that, in the systems considered for the calculations, the orbital  $|\Psi_{1L,2L}^A\rangle$  has a small amplitude [see Eqs. (64) and (66)]. In all the significant cases, the model accurately accounts for the numerical results.

We find that the states obtained from the numerical calculations include very small, but non-zero, contributions from some  $(J, M)$  components for which  $p_{k,J,M} = 0$  according to the model. We call  $h_k$  the sum of the weights of these  $(J, M)$  components beyond the Hubbard model for state  $k$ . For the singlet, we obtain  $h_1 \approx \{6, 5, 5\} \times 10^{-3}$  for the three considered values of  $a$ , respectively. The weights of the individual terms beyond Hubbard are all  $\lesssim 10^{-4}$ , except for  $p_{1,2,1} = p_{1,2,-1} = 1.3 \times 10^{-3}$  in all the three cases. For the triplet, we obtain  $h_2 \approx h_3 \approx h_4 \approx \{8, 6, 5\} \times 10^{-3}$  for the three values of  $a$ , respectively. The weights of the individual terms beyond Hubbard are all  $\lesssim 10^{-4}$ , except for  $p_{2,3,2} = p_{2,2,2} = p_{4,3,-2} = p_{4,2,-2}$ , which is equal to  $\approx \{3.5, 2.7, 2.5\} \times 10^{-3}$  for the three values of  $a$ , respectively.

One of the predictions of the Hubbard model in this four-band scenario is that both symmetric and antisymmetric two-hole orbitals contribute to the singlet and triplet states. The weight of the antisymmetric orbitals

quantity	$a = 5 \text{ nm}$	$a = 10 \text{ nm}$	$a = 14 \text{ nm}$
$p_{1,3,2} = p_{1,3,-2}$	$4 \times 10^{-3}$	$6 \times 10^{-3}$	$5 \times 10^{-3}$
$p_{2,2,1} = p_{4,2,-1}$	$16 \times 10^{-3}$	$12 \times 10^{-3}$	$10 \times 10^{-3}$
$p_{3,2,2} = p_{3,2,-2}$	$8 \times 10^{-3}$	$6 \times 10^{-3}$	$5 \times 10^{-3}$

TABLE V. Weights of the antisymmetric orbitals in the singlet and of the symmetric orbitals in the triplet.

in the singlet is given by the quantities  $p_{1,3,2} = p_{1,3,-2}$ , while the weight of the symmetric orbitals in the triplet is given by the quantities  $p_{2,2,1} = p_{4,2,-1}$  and  $p_{3,2,2} = p_{3,2,-2}$  [compare with Eqs. (63), (64), (65), (66)]. We report them in Table V for the same three cases considered above. In all cases, it is seen that the orbitals with minority symmetry have a total weight of the order of  $\approx 10^{-2}$ . The connection between this smallness and the small degree of spin-orbital entanglement is discussed in Section V.

- 
- \* [andrea.secchi@nano.cnr.it](mailto:andrea.secchi@nano.cnr.it)
- <sup>1</sup> G. Burkard, D. Loss, and D. P. DiVincenzo, *Phys. Rev. B* **59**, 2070 (1999).
  - <sup>2</sup> J. I. Climente, M. Korkusinski, G. Goldoni, and P. Hawrylak, *Phys. Rev. B* **78**, 115323 (2008).
  - <sup>3</sup> A. I. Yakimov, A. A. Bloshkin, and A. V. Dvurechenskii, *Phys. Rev. B* **81**, 115434 (2010).
  - <sup>4</sup> D. Loss and D. P. DiVincenzo, *Phys. Rev. A* **57**, 120 (1998).
  - <sup>5</sup> F. A. Zwanenburg, A. S. Dzurak, A. Morello, M. Y. Simmons, L. C. L. Hollenberg, G. Klimeck, S. Rogge, S. N. Coppersmith, and M. A. Eriksson, *Rev. Mod. Phys.* **85**, 961 (2013).
  - <sup>6</sup> G. Scappucci, C. Kloeffel, F. A. Zwanenburg, D. Loss, M. Myronov, J.-J. Zhang, S. De Franceschi, G. Katsaros, and M. Veldhorst, *Nature Rev. Mat.* (2020).
  - <sup>7</sup> K. Horibe, T. Kodera, and S. Oda, *Applied Physics Letters* **106**, 083111 (2015).
  - <sup>8</sup> Y. Yamaoka, S. Oda, and T. Kodera, *Applied Physics Letters* **109**, 113109 (2016).
  - <sup>9</sup> Y. Hada and M. Eto, *Japanese Journal of Applied Physics* **43**, 7329 (2004).
  - <sup>10</sup> L. Wang, K. Shen, B. Y. Sun, and M. W. Wu, *Phys. Rev. B* **81**, 235326 (2010).
  - <sup>11</sup> L. Wang and M. W. Wu, *Journal of Applied Physics* **110**, 043716 (2011).
  - <sup>12</sup> S. Das Sarma, X. Wang, and S. Yang, *Phys. Rev. B* **83**, 235314 (2011).
  - <sup>13</sup> C. B. Simmons, J. R. Prance, B. J. Van Bael, T. S. Koh, Z. Shi, D. E. Savage, M. G. Lagally, R. Joynt, M. Friesen, S. N. Coppersmith, and M. A. Eriksson, *Phys. Rev. Lett.* **106**, 156804 (2011).
  - <sup>14</sup> M. Raith, P. Stano, and J. Fabian, *Phys. Rev. B* **86**, 205321 (2012).
  - <sup>15</sup> E. Nielsen, R. Rahman, and R. P. Muller, *Journal of Applied Physics* **112**, 114304 (2012).
  - <sup>16</sup> T. F. Watson, S. G. J. Philips, E. Kawakami, D. R. Ward, P. Scarlino, M. Veldhorst, D. E. Savage, M. G. Lagally, M. Friesen, S. N. Coppersmith, M. A. Eriksson, and L. M. K. Vandersypen, *Nature* **555**, 633 (2018).
  - <sup>17</sup> D. M. Zajac, A. J. Sigillito, M. Russ, F. Borjans, J. M. Taylor, G. Burkard, and J. R. Petta, *Science* **359**, 439 (2018).
  - <sup>18</sup> F. Ansaloni, A. Chatterjee, H. Bohuslavskiy, B. Bertrand, L. Hutin, M. Vinet, and F. Kuemmeth, *Nat. Commun.* **11**, 6399 (2020).
  - <sup>19</sup> R. Maurand, X. Jehl, D. Kotekar-Patil, A. Corna, H. Bohuslavskiy, R. Lavi  ville, L. Hutin, S. Barraud, M. Vinet, M. Sanquer, and S. De Franceschi, *Nat. Commun.* **7**, 13575 (2016).
  - <sup>20</sup> S. Bonen, U. Alakusu, Y. Duan, M. J. Gong, M. S. Dadash, L. Lucci, D. R. Daughton, G. C. Adam, S. Iord  nescu, M. P  şteanu, I. Giangu, H. Jia, L. E. Gutierrez, W. T. Chen, N. Messaoudi, D. Harame, A. M  ller, R. R. Mansour, P. Asbeck, and S. P. Voinigescu, *IEEE Electron Device Letters* **40**, 127 (2019).
  - <sup>21</sup> B. Het  nyi, C. Kloeffel, and D. Loss, *Phys. Rev. Research* **2**, 033036 (2020).
  - <sup>22</sup> H. Watzinger, C. Kloeffel, L. Vuku  i  , M. D. Rossell, V. Sessi, J. Kuku  ka, R. Kirchschr  ger, E. Lausecker, A. Truhlar, M. Glaser, A. Rastelli, A. Fuhrer, D. Loss, and G. Katsaros, *Nano Letters* **16**, 6879 (2016).
  - <sup>23</sup> H. Watzinger, J. Kuku  ka, L. Vuku  i  , F. Gao, T. Wang, F. Sch  ffler, J.-J. Zhang, and G. Katsaros, *Nat. Commun.* **9**, 3902 (2018).
  - <sup>24</sup> N. W. Hendrickx, D. P. Franke, A. Sammak, G. Scappucci, and M. Veldhorst, *Nature* **577**, 487 (2019).
  - <sup>25</sup> N. W. Hendrickx, W. I. L. Lawrie, L. Petit, A. Sammak, G. Scappucci, and M. Veldhorst, *Nat. Commun.* **11**, 3478 (2020).
  - <sup>26</sup> L. A. Terrazos, E. Marcellina, Z. Wang, S. N. Coppersmith, M. Friesen, A. R. Hamilton, X. Hu, B. Koiller, A. L. Saraiva, D. Culcer, and R. B. Capaz, *Phys. Rev. B* **103**, 125201 (2021).
  - <sup>27</sup> S. Bosco, B. Het  nyi, and D. Loss, *PRX Quantum* **2**, 010348 (2021).
  - <sup>28</sup> Y. Hada and M. Eto, *Phys. Rev. B* **68**, 155322 (2003).
  - <sup>29</sup> L. Y. Voon and M. Willatzen, *The  $\mathbf{k} \cdot \mathbf{p}$  Method* (Springer-Verlag Berlin Heidelberg, 2009).
  - <sup>30</sup> C. Y.-P. Chao and S. L. Chuang, *Phys. Rev. B* **46**, 4110 (1992).
  - <sup>31</sup> D. V. Bulaev and D. Loss, *Phys. Rev. Lett.* **98**, 097202 (2007).
  - <sup>32</sup> A. Corna, L. Bourdet, R. Maurand, A. Crippa, D. Kotekar-Patil, H. Bohuslavskiy, R. Lavi  ville, L. Hutin, S. Barraud, X. Jehl, M. Vinet, S. De Franceschi, Y.-M. Niquet, and M. Sanquer, *npj Quantum Inf.* **4**, 6 (2018).
  - <sup>33</sup> P. Cerfontaine, T. Botzem, J. Ritzmann, S. S. Humpohl, A. Ludwig, D. Schuh, D. Bougeard, A. D. Wieck, and H. Bluhm, *Nat. Commun.* **11**, 4144 (2020).
  - <sup>34</sup> M. F. Doty, J. I. Climente, M. Korkusinski, M. Scheibner, A. S. Bracker, P. Hawrylak, and D. Gammon, (2008), [arXiv:0804.3097 \[cond-mat.mtrl-sci\]](https://arxiv.org/abs/0804.3097).
  - <sup>35</sup> A. I. Yakimov, V. A. Timofeev, A. I. Nikiforov, and A. V. Dvurechenskii, *JETP Letters* **94**, 744 (2012).
  - <sup>36</sup> K. Deng, F. A. Calderon-Vargas, N. J. Mayhall, and

- E. Barnes, [Phys. Rev. B \*\*97\*\*, 245301 \(2018\)](#).
- <sup>37</sup> J. M. Luttinger and W. Kohn, [Phys. Rev. \*\*97\*\*, 869 \(1955\)](#).
- <sup>38</sup> A. Secchi, L. Bellentani, A. Bertoni, and F. Troiani, (2020), [arXiv:2010.01332 \[cond-mat.mes-hall\]](#).
- <sup>39</sup> B. Venitucci, L. Bourdet, D. Pouzada, and Y.-M. Niquet, [Phys. Rev. B \*\*98\*\*, 155319 \(2018\)](#).
- <sup>40</sup> J. Hubbard, [Proc. R. Soc. Lond. A \*\*276\*\*, 238 \(1963\)](#).